NRL Report 6864

An Analysis of the Forces and Bending Moments Generated During the NRL Dynamic Tear Test

G. E. Nash

Metallurgy Division

January 30, 1969

NAVAL RESEARCH LABORATORY
Washington, D.C.

This document has been approved for public release and sale; its distribution is unlimited.

CONTENTS

Abstract..... ii
Problem Status..... ii
Authorization..... ii

NOTATION.....iii

INTRODUCTION..... 1

HAMMER FORCES AND SPECIMEN BENDING MOMENTS.. 4

COMPARISON WITH EXPERIMENTAL RESULTS AND
CALCULATION OF THE TEAR ENERGY.....12

CONCLUSIONS AND SUGGESTIONS FOR FUTURE WORK.26

NOTE ADDED IN PROOF.....28

REFERENCES.....29

APPENDIX I.....31

APPENDIX II.....51

TABLE I.....54

TABLE II.....55

FIGURES 1 THROUGH 21 56

ABSTRACT

An analysis is presented which predicts the hammer forces, specimen bending moments, and tear energies generated during the NRL Dynamic Tear test. The theoretical predictions agree quite well with experimental observations for relatively brittle materials.

The tear energy per unit net area calculated from this analysis is shown to vary significantly with initial impact velocity and specimen length for a brittle material. It is relatively independent of the specimen thickness and notch depth to width ratio.

PROBLEM STATUS

An interim report on the problem, work is continuing.

AUTHORIZATION

NRL Problem Number: M01-25

Project Number: RR007-01-46-5432

Manuscript submitted November 26, 1968.

NOTATION

a - Notch depth

A_g - Cross sectional area of gross section

A - Beam cross sectional area

B_1 - Portion of the boundary over which displacements are prescribed

B_2 - Portion of the boundary over which tractions are prescribed

b - Beam thickness

d - Unbroken ligament depth

E - Young's modulus

F - Hammer force

F_i - Body force vector

f_i - $[t*F_i] + \rho[t\dot{u}_i(0,\underset{\sim}{x}) + u_i(0,\underset{\sim}{x})]$

G - Shear modulus

$\mathcal{G}_I$ - Mode I fracture toughness

h - Beam half height

H - Heaviside unit step function

I - Cross sectional moment of inertia about the c.g.

I_g - Moment of inertia of the gross section

I'' - Moment of inertia of equivalent uniform beam

k_1 - $\frac{1}{m_1} + \frac{1}{m_2}$

k_2 - Constant in the Hertz Theory of Contact Forces

k_4 - Constant in the assumed linear contact theory

K_I - Mode I stress intensity factor

K_t - Elastic stress concentration factor

L - Beam length

M - Bending moment

m_1 - Hammer mass

m_2 - Anvil mass

p - Applied load per unit length on the top surface of the beam; also the Laplace transform parameter

R - Bounded region of Euclidean 3-space; also notch root radius

$\hat{T}_i$ - Prescribed surface traction on B_2

$\hat{u}_i$ - Prescribed displacement vector on B_1

u_i - Displacement vector

u_y - Beam deflection referred to the embedded coordinates x_i

V - Shear force

V_1 - Hammer velocity referred to the fixed coordinates X_i

V_2 - Rigid body beam velocity referred to the fixed coordinates X_i

V_{01}, V_{02} - Initial hammer or rigid body beam velocity

X_1 - Hammer displacement referred to the fixed coordinates

X_2 - Rigid body beam displacement referred to the fixed coordinates

X_{01}, X_{02} - Initial hammer or rigid body beam displacements

$\underset{\sim}{x}$ - Point (x,y,z) in Euclidean 3-space

$Y_i(\xi)$ - Eigenvector of the beam equations

α - Relative approach in Hertz theory

δ - Measure of the influence of the local stress field of the notch; also Dirac delta function

$\underset{\sim}{\epsilon} = \epsilon_{ij}$ - strain tensor

$\underset{\sim}{\tau} = \tau_{ij}$ - stress tensor

κ_{ijkl} - Elastic compliance tensor, i.e., $\epsilon_{ij} = \kappa_{ijkl}\,\tau_{kl}$

ρ - Mass density

ω_i - Eigenvalues of the beam equations (natural frequencies)

AN ANALYSIS OF THE FORCES AND BENDING MOMENTS GENERATED DURING THE NRL DYNAMIC TEAR TEST

INTRODUCTION

Traditionally, notched beam impact tests have been used to determine a material's resistance to fracture based on energy considerations. Until recently, no attempt has been made to obtain more fundamental information such as the bending moments and stresses in the beam during impact. Admittedly, this is a most complex problem. When one considers the scarcity of dynamical solutions in bounded media with simple boundaries (for example, no exact solution has been found yet for the flexure of a cylindrical bar of finite length), the introduction of a notch seems to introduce almost insurmountable difficulties. Be that as it may, a knowledge of the beam stresses during impact is of considerable interest to those concerned with fracture mechanics since once these stresses are determined, dynamic stress intensity factors may be computed.

This report concerns the development of a systematic method for predicting the impact force and bending moment-time responses generated during the NRL Dynamic Tear test. It is presented in two main sections. The first section is devoted to theoretical considerations. The second section is concerned with the experimental verification of the analysis and its applications.

In the first section, the approach used parallels the standard method for treating transverse impact problems [1]; however there are several important differences. Obviously, the presence of a notch precludes the direct application of the one dimensional flexure theories commonly used in uniform beam impact problems. The bending moments and deflections in a notched beam must therefore be found from either a two dimensional dynamical solution or a refined one dimensional theory which takes into account the effect of the local stress distribution near the notch. Also, the previous investigations had as their primary objective the determination of pulse shapes, dispersion relations, etc., and were not concerned with the effect of specimen cracking on the load-time curve (the loads were kept low enough so this did not occur).

In this investigation, a refined one dimensional bending theory is devised using a variational principle proposed by Gurtin [2]. The details of this calculation are shown in Appendix I. Using these results, an integral equation is derived for the hammer force as a function of time and solved in closed form by Laplace transforms. The closed form solution, however, requires the assumption of a single active bending mode. The influence of the higher modes is evaluated in Appendix II and an iterative procedure is described with which the hammer force can be obtained to any degree of precision desired.

The effects of specimen cracking are accounted for in a straight forward manner by approximating the crack length-time relation by a series of steps and solving the integral equation for the hammer force in each time interval corresponding to a constant crack length. The effects of localized plasticity at the contact point and gross yielding of the specimen are neglected. The analysis is thus limited to relatively brittle materials at this time. Once the hammer force is known as a function of time, the bending moment at any point in the specimen may be calculated from the relation derived in Appendix I.

In the second section of the report, the results of the theoretical analysis are compared to the experimental results obtained for two types of Dynamic Tear test specimens. The first is 5/8 x 1-5/8 x 7 inches and is designed for use in the 2,000 ft-lb, double pendulum impact machine. The second measures 6-3/8 x 12 x 58 inches and is used with the 160,000 ft-lb drop weight machine. A typical Dynamic Tear test specimen is shown in Fig. 1. The double pendulum and drop weight impact machines are shown in Figs. 2 and 3. The experimental results are obtained by the procedure described in [3].

Finally, in the second section several series of calculations are performed in which the tear energies (which may be calculated directly from the force-time response) are

tabulated for specimens with varying lengths, thicknesses, notch depths and initial impact velocities. The material is assumed to be brittle with a $K_{Icd} \cong 100$ ksi$\sqrt{\text{in}}$. It is found that the tear energy per unit fracture area is relatively constant when the thickness and notch depth are changed but varies considerably with the length and initial impact velocity.

HAMMER FORCES AND SPECIMEN BENDING MOMENTS

Consider the rigid body motion of the hammer. Applying Newton's second law and integrating twice gives:

$$X_1 = -\frac{1}{m_1}\int_0^t F(\eta)(t-\eta)d\eta + V_{01}t + X_{01} \tag{1}$$

Similarly, applying the second law to the beam to account for the rigid body motion gives:

$$X_2 = +\frac{1}{m_2}\int_0^t F(\eta)(t-\eta)d\eta + V_{02}t + X_{02} \tag{2}$$

where $V_{02}t$ is assumed $\gg \frac{1}{m_2}\int_0^t F(\eta)(t-\eta)d\eta$ during the initial stages of impact for the double pendulum machine, For the drop-weight machine, $m_2 = \infty$ and $V_{02} = 0$. The coordinate system used here is shown in Fig. 4.

Since the beam is also bending elastically, the total beam displacement at $X = L/2$ is:

$$X_t = X_2 + u_y(L/2,t) \tag{3}$$

When certain restrictions are imposed on the notch stresses (see Appendix I), it can be shown that:

$$u_y = \sum_{i=1}^{\infty} (A_i \sin\omega_i t + B_i \cos\omega_i t)\, Y_i(\xi) +$$

$$+ \sum_{i=1}^{\infty} \frac{Y_i(\xi) Y_i(1/2)}{\omega_i W_i} \int_0^t F(\eta) \sin\omega_i (t-\eta) d\eta \tag{4}$$

where

$$W_i \equiv \rho A_g \int_0^1 Y_i^2(\xi) d\xi$$

The eigenvalues ω_i and the eigenvectors $Y_i(\xi)$ are presumed known; the coefficients A_i and B_i may be found from the following relations which are easily derived from the orthogonality condition on the eigenvectors stated in Appendix I:

$$\omega_i A_i = \frac{1}{W_i} \rho A_g \int_0^1 \dot{u}_y(\xi,0) Y_i(\xi) d\xi$$

$$B_i = \frac{1}{W_i} \rho A_g \int_0^1 u_y(\xi,0) Y_i(\xi) d\xi \tag{5}$$

When the vibrations of the hammer and anvil are neglected, the following relation must hold at the contact point due to displacement continuity conditions:

$$X_1 - X_t = \alpha \tag{6}$$

where $\alpha = \alpha(F)$

For simplicity, a linear relation between F and α will be assumed in the form:

$$\alpha = F/k_4 \tag{7}$$

where k_4 is an experimentally determined constant. In reality, the F-α relationship is generally non-linear. For purely elastic deformation at the contact point, the Hertz contact theory predicts a reationship of the form:

$$F = k_2\alpha^{3/2} \tag{8}$$

When plasticity effects are taken into account, a relationship of the form:

$$F = N\alpha^{q} \tag{9}$$

is usually postulated where N and q are constants. For a full discussion, see Goldsmith [4].

Returning to equation (6) and substituting equations (1), (2), (3), (4), and (7) we have:

$$\begin{aligned} F/k_4 = {} & (V_{01}-V_{02})t + (X_{01}-X_{02}) - k_1\int_0^t F(\eta)(t-\eta)d\eta - \\ & - \sum_{i=1}^{\infty}(A_i\sin\omega_i t + B_i\cos\omega_i t)Y_i(1/2) - \\ & - \sum_{i=1}^{\infty}\frac{Y_i^{\,2}(1/2)}{\omega_i W_i}\int_0^t F(\eta)\sin\omega_i(t-\eta)d\eta \end{aligned} \tag{10}$$

The solution of (10) should yield the force-time relation during impact provided the specimen does not crack.

Now let us assume that a crack initiates at the notch root at time $t=t_1$, and then proceeds to propagate through the specimen cross section. If the crack length-time relation can be approximated by a series of discontinuous

jumps with d_o the unbroken ligament depth for $t \epsilon [t_o, t_1]$; etc., then Y_i, ω_i, etc., will be step functions in time. Let Y_{ik}, ω_{ik}, etc., denote the constant value of Y_i, ω_i etc., in the interval $[t_k, t_{k+1}]$ for $k = 0, 1, 2, \ldots, K$. Then equation (10) can be written as a set of K+1 integral equations in $F_k(\tau)$ where $F_k(\tau) \equiv F(t)$, $t \epsilon [t_k, t_{k+1}]$ and $\tau \equiv t - t_k$. Thus we have:

$$\frac{1}{k_4}(F_k - F_{0k}) + \alpha_{0k} = (V_{01} - V_{02})_k \, \tau + (X_{01} - X_{02})_k -$$

$$- k_1 \int_0^{\tau} F_k(\tau)(\tau - \eta) d\eta - \sum_{i=1}^{\infty} (A_{ik} \sin\omega_{ik}\tau + B_{ik} \cos\omega_{ik}\tau) Y_{ik}(1/2) -$$

$$- \sum_{i=1}^{\infty} \frac{Y_{ik}^2 (1/2)}{\omega_{ik} W_{ik}} \int_0^{\tau} F_k(\eta) \sin\omega_{ik}(\tau - \eta) d\eta \tag{11}$$

for

$$t \epsilon [t_k, t_{k+1}], \; k = 0, 1, 2, \ldots K$$

where

$$(X_{01} - X_{02})_k \equiv X_{1k-1}(t_k) - X_{2k-1}(t_k)$$

$$(V_{01} - V_{02})k \equiv \frac{d}{d\tau} X_{1k-1}(t_k) - \frac{d}{d\tau} X_{2k-1}(t_k) \tag{12}$$

$$\omega_{ik} A_{ik} \equiv \frac{1}{W_{ik}} \rho A g \int_0^1 \dot{u}_{yk-1}(\xi, t_k) Y_{ik} d\xi$$

$$B_{ik} \equiv \frac{1}{W_{ik}} \rho A g \int_0^1 u_{yk-1}(\xi, t_k) Y_{ik} d\xi$$

$$\alpha_{0k} \equiv \alpha_{k-1}(t_k)$$

$$F_{ok} \equiv F_{k-1}(t_k)$$

and

$$X_{1k-1}(t_k) - X_{2k-1}(t_k) = - k_1\int_0^{(t_k-t_{k-1})} F_{k-1}(\eta)[t_k-t_{k-1})-\eta]d\eta +$$

$$+ (V_{01}-V_{02k-1})(t_k-t_{k-1}) + (X_{01}-X_{02})_{k-1}$$

$$\frac{d}{d\tau}[X_{1k-1}(t_k)-X_{2k-1}(t_k)] = k_1\int_0^{(t_k-t_{k-1})} F_{k-1}(\eta)d\eta + (V_{01}-V_{02})_{k-1}$$

$$u_{yk-1}(\xi,t_k) = \sum_{i=1}^{\infty}[A_{ik-1}\sin\omega_{ik-1}(t_k-t_{k-1}) +$$

$$+ B_{ik-1}\cos\omega_{ik-1}(t_k-t_{k-1})]Y_{ik-1}(\xi) + \sum_{i=1}^{\infty}\frac{Y_{ik-1}(\xi)Y_{ik-1}(1/2)}{\omega_{ik}W_{ik-1}} \times$$

$$\times\int_0^{(t_k-t_{k-1})} F_{k-1}(\eta)\sin\omega_{ik-1}\ [(t_k-t_{k-1})-\eta]d\eta \tag{13}$$

$$\dot{u}_{yk-1}(\xi,t_k) = \sum_{i=1}^{\infty}[A_{ik-1}\cos\omega_{ik-1}(t_k-t_{k-1}) -$$

$$- B_{ik}\sin\omega_{ik-1}\ (t_k-t_{k-1})]\omega_{ik-1}Y_{ik-1}(\xi) +$$

$$+ \sum_{i=1}^{\infty}\frac{Y_{ik-1}(\xi)Y_{ik-1}(1/2)}{W_{ik-1}} \times$$

$$\times \int_0^{(t_k-t_{k-1})} F_{k-1}(\eta)\cos\omega_{ik-1}\ [(t_k-t_{k-1})-\eta]d\eta$$

$$(K = 1,2,.....K)$$

The values $(X_{01}-X_{02})_0$, $(V_{01}-V_{02})_0$, U_{y0}, F_{00} and α_{00} are given as initial conditions. In the problem at hand, $(X_{01}-X_{02})_0 = u_{yo} = \dot{u}_{y0} = F_{00} = \alpha_{00} = 0$.

We now consider solutions to equation (11). The usual approach in previous transverse impact investigations has been the small increment technique developed by Timoshenko [5].

This consists of approximating the integrals by summations thus reducing the solution of the integral equations to the solution of a set of linear algebraic equations. This technique will not be used here; instead, as a first approximation, we assume that all bending modes higher than the first are negligible, i.e., $Y_{ik} = 0$ ($i = 2, 3, \ldots$). Equations (11) now reduce to a fairly simple set of linear integral equations which may be solved in closed form by Laplace transforms. Appendix II deals with a technique by which we can assess the validity of this assumption and correct for the presence of the higher bending modes if necessary. Thus the disadvantage of this technique compared with Timoshenkos' is the linear F-α relation which we must assume while the advantage is the availability of a closed form solution as a first approximation of F(t).

Letting $Y_{ik}(\xi) = 0 (i=2,3,\ldots)$, we have from (11):

$$\frac{1}{\bar{k}_4}(F_k - F_{0k}) + \alpha_{ok} = (V_{01}-V_{02})_k\tau + (X_{01}-X_{02})_k - \\ - k_1\int_0^\tau F_k(\eta)(t-\eta)d\eta - (A_{1k}\sin\omega_{1k}\tau + B_{1k}\cos\omega_{1k}\tau)Y_{1k}(1/2) - \\ - \frac{Y_{1k}^2(1/2)}{\omega_{1k}W_{1k}}\int_0^\tau F_k(\eta)\sin\omega_{1k}(\tau-\eta)d\eta \tag{14}$$

Taking the Laplace transform of (14) and solving for $\bar{F}_k(p)$ where $\bar{F}_k(p) = \mathcal{L}\{F(t)\}$ and p is the transform parameter, we have:

$$\bar{F}(p) = k_4(V_{01}-V_{02})_k \left[\frac{p^2+\omega_{1k}^2}{p^4+\Theta_k p^2+\Psi_k}\right] - k_4(A_1\omega_1 Y_1(1/2))_k \times$$

$$\times \left[\frac{p^2}{p^4+\Theta_k p^2+\Psi_k}\right] - k_4(B_1 Y_1(1/2))_k \left[\frac{p^3}{p^4+\Theta_k p^2+\Psi_k}\right] +$$

$$+ k_4[(X_{01}-X_{02})_k - \alpha_{ok} + \frac{F_{ok}}{k_4}] \left[\frac{p(p^2+\omega_{1k}^2)}{p^4+\Theta_k p^2+\Psi_k}\right] \tag{15}$$

where

$$\Theta_k \equiv \omega_{1k}^2 + k_1 k_4 + k_{3k} k_4, \qquad \Psi_k \equiv k_1 k_4 \omega_{1k}^2$$

$$k_{3k} \equiv \frac{Y_{1k}^2(1/2)}{W_{1k}}$$

Equation (15) may be easily inverted by use of the tables in Roberts and Kaufman [6]. This gives

$$F_k(\tau) = \frac{k_4}{(\alpha^2-\beta^2)_k} \left\{\frac{(V_{01}-V_{02})_k}{(\alpha\beta)_k} [\alpha_k(\omega_{1k}^2-\beta_{1k}^2)\sin\beta_k\tau + \right.$$

$$+ \beta_k(\alpha^2{}_k-\omega_{1k}^2)\sin\alpha_k\tau] - [A_1\omega_1 Y_1(1/2)]_k [\alpha_k \sin\alpha_k\tau - \beta_k \sin\beta_k\tau] -$$

$$- [B_1 Y_1(1/2)]_k [\alpha^2{}_k \cos\alpha_k\tau - \beta^2{}_k \cos\beta_k\tau] + \tag{16}$$

$$+ [(X_{01}-X_{02})_k - \alpha_{0k} + \frac{F_{0k}}{k_4}] [(\omega_{1k}^2-\beta_k^2)\cos\beta_k\tau +$$

$$\left. + (\alpha_k^2-\omega_{1k}^2)\cos\alpha_k\tau]\right\}$$

where $\alpha^2{}_k \equiv \dfrac{\Theta^2{}_k + \sqrt{\Theta_k^2-4\Psi_k}}{2}$, $\beta^2{}_k \equiv \dfrac{\Theta_k - \sqrt{\Theta_k^2+4\Psi_k}}{2}$

and $\tau = t - t_k$, $t \in [t_k, t_{k+1}]$

Note here that since $u_{yk}(\xi,\tau)$ is taken in the form:

$$u_{yk}(\xi,\tau) = (A_{1k}\sin\omega_{1k}\tau + B_{1k}\cos\omega_{1k}\tau)Y_{1k}(\xi) +$$

$$+ \frac{Y_{1k}(\xi)Y_{1k}(1/2)}{\omega_{1k}W_{1k}} \int_{0\,k-1}^{\tau} F(\eta)\sin\omega_{1k}(\tau-\eta)d\eta \tag{17}$$

A_{1k} and B_{1k} are now given by:

$$\omega_{1k}A_{1k} = \frac{\dot{u}_{yk-1}(\xi,t_k)}{Y_{1k}(\xi)}$$

$$B_{1k} = \frac{u_{yk-1}(\xi,t_k)}{Y_{1k}(\xi)} \tag{18}$$

rather than (12).

Now that the hammer force-time relation is known, the calculation of the specimen bending moment and the hammer energy loss (tear energy) follows directly. For the bending moments, we have from the results of Appendix I:

$$\frac{-E}{L^2\Phi_1}\frac{\partial^2 u_y}{\partial\xi^2} = M(\xi,t) \tag{19}$$

substituting equation (4) into (19), we have:

$$M_k = \frac{-E}{L^2\Phi_1}\left\{\sum_{i=1}^{\infty}(A_{ik}\sin\omega_{ik}\tau + B_{ik}\cos\omega_{ik}\tau)\frac{d^2}{d\xi^2}Y_{ik}(\xi) +\right.$$

$$\left. + \sum_{i=1}^{\infty}\frac{d^2}{d\xi^2}\frac{Y_{ik}(\xi)Y_{ik}(1/2)}{\omega_{ik}W_{ik}}\int_0^{\tau}F_k(\eta)\sin\omega_{ik}(\tau-\eta)d\eta\right\} \tag{20}$$

for

$$t\in[t_k,\ t_{k+1}],\ \tau = t - t_k$$

The tear energy, ΔE, is easily found as a function of $F(t)$ by applying the impulse-momentum relation and the conservation of energy. Thus we have:

$$\Delta E = Q[(V_{01}-V_{02}) - \frac{Q}{m_I}] \text{ for the double pendulum} \tag{21a}$$

$$\Delta E = Q[(V_{01}-V_{02}) - \frac{Q}{2m_I}] \text{ for the drop weight} \tag{21b}$$

where $Q \equiv \int_0^t F(\eta)d\eta$

COMPARISON WITH EXPERIMENTAL RESULTS AND CALCULATION OF THE TEAR ENERGY

In this section, the results of the analysis are compared to the experimental results for the 5/8 inch DT specimen (6001 aluminum and J-22 steel at room temperature) and the 6-3/8 in DT specimen (L-14 steel at 70°F and 120°F). Also, calculations for the force-time response and tear energies are presented for the J-22 steel as a function of various geometrical parameters and the initial impact velocities.

Because of the computational difficulties involved, some simplifying assumptions were made so that the numerical could be carried out in a convenient fashion. First of all, the iteration procedure outlined in Appendix II for including the effects of the higher order bending modes in the integral equation for the force-time response is not employed. Second, the eigenvalues and eigenvectors of the beam field equations are assumed to be given as:

$$Y_{ik}(\xi) = \sin i\pi\xi$$

$$\omega_{ik} = \left(\frac{i\pi}{L}\right)^2 \sqrt{\frac{EI_k''}{\rho A_g}} \tag{22}$$

where I_k'' is a fictitous moment of inertia and is a function of a/2h. The eigenvalues and eigenvectors were assumed in this form because the solution to the beam field equation outlined in the last part of Appendix I was not yet complete at the time these calculations were performed. Equation (22) is just a modified version of the familiar result for a simply supported, Euler-Bernoulli beam. I_k'' is estimated as follows:

From the compliance- crack length relation [7], we have:

$$b\mathcal{G}_I = \frac{1}{2} F^2 \frac{d}{da}\left(\frac{u_y(L/2)}{F}\right) \tag{23}$$

for a beam with a statically applied load F at midspan. $\mathcal{G}$ = is the mode I fracture toughness and a = 2h-d. But:

$$K_I^2 = E\mathcal{G}_I \tag{24}$$

where K_I is the mode I stress intensity factor and from the results of [8] for static three point bending, we have:

$$K_I^2 = \frac{\chi^2 F^2 L^2}{16(2h)^3 b^2} \tag{25}$$

where

$$\chi^2 = 130(a/2h) - 263(a/2h)^2 + 820\ (a/2h)^3 \tag{26}$$

Therefore, upon substituting (24), (25), and (26) into (23) and integrating, we get:

$$u_y(L/2) = \frac{FL^3}{48EI_g}\left[1+\frac{h}{L}(65(a/2h)^2-87.3(a/2h)^3+205(a/2h)^4\right] \tag{27}$$

Since the deflection at midspan for a uniform beam with a moment of inertia I" is given as:

$$u_y(L/2) = \frac{FL^3}{48EI''} \tag{28}$$

we have:

$$I'' = \frac{I_g}{1+\frac{h}{L}[65(a/2h)^2-87.3(a/2h)^3+205(a/2h)^4]} \tag{29}$$

Curves showing I" as a function of a/2h are displayed for the two DT specimens in Figs. 5 and 6.

Now that $Y_{ik}(\xi)$ and ω_{ik} are determined, the forces and bending moments may be calculated. From (22) and (16), we have:

$$\begin{aligned} F_k(\tau) = \frac{k_4}{(\alpha^2-\beta^2)_k}\Bigg\{ & \frac{(V_{01}-V_{02})_k}{(\alpha\beta)_k}\ [\alpha_k(\omega_{1k}{}^2-\beta_k{}^2)\sin\beta_k\tau + \\ & + \beta_k(\alpha_k{}^2-\omega_{1k}{}^2)\sin\alpha_k\tau] - A_{1k}\omega_{1k}[\alpha_k\sin\alpha_k\tau - \beta_k\sin\beta_k\tau] - \\ & -B_{1k}\ [\alpha_k{}^2\cos\alpha_k\tau - \beta_k{}^2\cos\beta_k\tau] + \\ & + [(X_{01}-X_{02})_k - \alpha_{0k} + \frac{F_{0k}}{k_4}]\ [(\omega_{1k}{}^2-\beta_k{}^2)\cos\beta_k\tau + \\ & + (\alpha_k{}^2-\omega_{1k}{}^2)\cos\alpha_k\tau]\Bigg\} \end{aligned} \tag{30}$$

for $t\in[t_{k1}t_{k+1}]$, $k = 0,1,2,\ldots,K$

The coefficients A_{1k}, B_{1k} are found from expressions (17) and (18):

$$(A_1\omega_1)_k = (A_1\omega_1)_{k-1}\cos\omega_{1k-1}(t_k-t_{k-1}) - (B_1\omega_1)_{k-1}$$

$$\sin\omega_{1k-1}(t_k-t_{k-1}) + k_3\int_0^{(t_k-t_{k-1})} F_{k-1}(\eta)\cos\omega_{1k-1}[(t_k-t_{k-1})-\eta]d\eta \tag{31}$$

$$B_{1k} = A_{1k-1}\sin\omega_{1k-1}(t_k-t_{k-1}) + B_{1k-1}\cos\omega_{1k-1}(t_k-t_{k-1}) +$$

$$+ \frac{k_3}{\omega_{1k-1}}\int_0^{(t_k-t_{k-1})} F_{k-1}(\eta)\sin\omega_{1k-1}[(t_k-t_{k-1}) - \eta]d\eta$$

also, $k = 1,2,\ldots,K$ $\quad (X_{01}-X_{02})_k - \alpha_{ok} = u_{yk-1}(\xi,t_k) = B_{1k}$ (32)

and $A_{10} = B_{10} = F_{00} = 0$.

The bending moment prior to fracture initiation, i.e., $t\epsilon[t_0, t_1]$, is easily found from equations (20) and (22).

$$M_0(\xi,t) = \left(\frac{2}{\rho A_g}\right) EI''_0\left(\frac{\pi}{L}\right)^2 \sum_{i=1,3,5\ldots}^{\infty} \frac{i^2}{\omega_{1k}} \sin\frac{i\pi}{2} \sin i\pi\xi \;\times$$

$$\times\int_0^t F_0(\eta)\sin\omega_{10}(t-\eta)d\eta \tag{33}$$

Substituting equation (30) in (33), we have:

$$M_0(\xi,t) = P_0\left[\frac{(\omega_1^2-\beta^2)_0}{\beta_0} \sum_{i=1,3,5..}^{\infty} \frac{\beta_0\sin\omega_{i0}t-\omega_{i0}\sin\beta_0 t}{(\beta^2-\omega_i^2)_0} \times\right. \tag{34}$$

$$\times\sin\frac{i\pi}{2}\sin i\pi\xi + \frac{(\alpha^2-\omega_1^2)_0}{\alpha_0} \sum_{i=1,3,5}^{\infty} \frac{\alpha_0\sin\omega_{i0}t-\omega_{i0}\sin\alpha_0 t}{(\alpha^2-\omega_i^2)_0}\times$$

$$\left.\times\sin\frac{i\pi}{2}\sin i\pi\xi\right]$$

where

$$P_0 \equiv \frac{2k_4\omega_{10}L(V_{01}-V_{02})_0}{(\alpha^2-\beta^2)_0\pi^2}$$

It should be mentioned at this point that equation (33) has been found to converge fairly slowly and the integration for large values of i, if done numerically, presents some difficulties due to the oscillation of the term $\sin\omega_{i0}(t-\eta)$. One of the primary advantages of the iteration technique described in this paper for the solution of (11) is that the integration in (33) may be carried out analytically, thus avoiding this problem.

Figures 7 and 8 show the theoretical and experimental force-time and specimen bending moment-time (mid and quarter span) responses for 5/8 inch J-22 steel specimen. Looking at the midspan bending moment-time response (Fig. 8), it is seen that fracture occurred at ~70μsec. Since this material is brittle at room temperature (this was seen to be the case upon examination of the fracture surface), it can be assumed that once the crack initiated, it propagated very rapidly without arrest through the entire specimen. For the theoretical calculation of the impact force-time response, t_1 is therefore taken as 70μsec and the crack speed is assumed to be roughly 3000 ft/sec. K is taken as 3 with t_2 = 80μsec, t_3 = 90μsec, t_4 = 200μsec.

As can be seen in Fig. 7, the agreement between the theoretical and experimental results is excellent. The principle feature of these curves is that the peak load occurs prior to crack initiation. It is caused only by inertia effects and is unrelated to the fracture process.

Returning to Fig. 8, we note the excellent agreement for the bending moments at mid and quarter span. The presence of the compression region for the first 40μsec at quarter span is again an inertia effect.

Finally, Fig. 9 shows the theoretical bending moment at mid span for the J-22 steel along with a quasistatic midspan bending moment obtained from the hammer force, i.e.

$$M = \frac{FL}{4} \tag{35}$$

t_1 is allowed to approach infinity so that the material is now considered to be infinitely strong. We note here that after approximately 200μsec, the difference between the static and dynamic bending moments is relatively minor. (The actual difference is less than is indicated in the Figure due to damping effects which are not accounted for in the analysis.) Thus these curves show rather nicely the time range over which inertia effects must be considered in the calculation of the midspan bending moment. Since in the case under consideration, t_1 = 70μsec, the fracture moment cannot be calculated using equation (35) but must be obtained from the dynamic analysis (equation (34)).

Let us now examine the data for the 5/8 inch 6001 aluminum. The experimental and theoretical force-time and moment-time responses are shown in Figs. 10 and 11. We first note that the hammer force-time response (Fig. 10) is characterized by the occurrence of multiple peaks. However, if we calculate the force-time response from equation (30) for an infinitely strong specimen ($t_1 \rightarrow \infty$), we see that only a single peak at $t = 60\mu sec$ is predicted (see Fig. 10). This implies that the subsequent peaks occur during the crack propagation stage of the impact process but that the first peak is an inertia effect.

This inference is substantiated upon examination of the $M(1/2,t)$ - time responses shown in Fig. 11. Here we see that that strain gage response increases monotonically until $t = 120\mu sec$ where it decreases slightly and then goes off scale at $140\mu sec$. Since the theoretical calculation does not predict a decrease at $120\mu sec$ it may be assumed that it is due to crack iniation. At $t = 140\mu sec$, the crack has progressed through the strain gage. Going back to the force-time curve, we note a second peak at $140\mu sec$. This peak is caused by the decrease in specimen rigidity due to the presence of the crack. Subsequent peaks are caused by both crack propagation and inertia effects.

Figure 10 shows the theoretical force-time response calculated from equation (30) assuming a 50% pop-in at 3000 ft/sec and subsequent slow tearing at 50 ft/sec. t_1 is taken as 120μsec. Note that the second peak is now predicted by the theoretical analysis. The results are not shown for times greater than 350μsec because the agreement was quite poor. This is due to the effects of gross specimen yielding which become important at the later times. The discrepancy in the theoretical and experimental results for times less than 350μsec is thought to be due to localized yielding at the contact point. This introduces a path dependence on the constant k_4 (different for loading and unloading) and thus shifts the theoretical response along the time axis after the first peak.

Finally, Fig. 11 shows the bending moments at mid and quarter span prior to crack initiation. The agreement is quite good. Inertia effects again show up in the quarter span response, just as in the steel specimen. Since the time dependence in the initial portion of the force-time response is similar to that of the steel, we may infer from the results shown in Fig. 9 that inertia effects again must be considered for times less than approximately 200μsec. Since $t_1 \cong 120$μsec, the bending moment at fracture cannot be calculated using equation (35).

The analysis of the data for the 6-3/8 inch L-14 steel specimens is similar to the smaller specimens just discussed. Figure 12 shows the theoretical and experimental force-time response for 70°F. The material was observed to behave in a brittle manner and t_1 was found to be approximately 400μsec from strain gage records which are not shown here.

The theoretical curve was calculated assuming a crack speed of 3000 ft/sec. As can be seen from Fig. 12, the agreement is quite good. The outstanding feature of these results is that there exists a delay time of about 300μsec between fracture initiation and the peak in the force-time response. (This type of behavior was also observed in the 5/8 inch 6061 aluminum specimens, Fig. 9, but was not discussed explicitly.) The existence of the delay time is expected physically since the decrease in specimen rigidity due to crack extension must be quite large before the load actually starts to drop. The presence of the delay time is important in that it complicates the determination of t_1 from the force-time response.

Figures 13 and 14 show the force-time and bending moment-time responses for L-14 steel at 120°F. The fracture surface was primarily flat but there was evidence of a slight degree of shear lip formation. The response from gage 3, shown in Fig. 14, indicates crack initiation at 800 μ sec.

Figure 13 shows the theoretical and experimental force-time response. For the theoretical calculation, t_1 is taken as 800μsec and the crack speed is assumed to be 1500 ft/sec. The agreement is good although a time shift (as in the 6061 aluminum) is present.

Figure 14 shows the experimental bending moments at three locations on the specimen as indicated in the sketch. Also presented are the theoretical bending moments at mid and quarter span. The agreement at quarter span is excellent. The agreement between the response of gage 3 (three inches from midspan) and the theoretical bending moment response at mid span is excellent for times less than 350μsec. For times greater than this, the experimental results are significantly higher than the theoretical values. This disagreement is accounted for by the presence of the brittle crack starter.

Unlike the 5/8 inch specimen, the 6-3/8 inch specimens do not have a completely machined notch but rather a machined notch extending down 1 inch plus a brittle weld to act as a crack starter extending down 2 inches. Strain gage 3 was calibrated prior to the introduction of the brittle weld; hence the calibration is only valid for times less than the weld fracture time. Since a considerable disturbance was indicated at 350μsec on the experimental gage 3 - time response (not shown in Fig. 14), we can assume that the weld

fractured at that time. This accounts for the discrepancy between the theoretical and experimental results for times greater than 350μ. An estimate of the midspan bending moment can not be made from the other gage responses since the moment distribution along the beam axis can not be assumed linear in the time interval of interest.

Finally, Fig. 15 shows the theoretical dynamic and quasistatic bending moments at midspan for the L-14 steel assuming the material has infinite fracture strength. Inertia effects become relatively minor after approximately 2 m.sec. In both tests on the L-14 steel just discussed, fracture occurs prior to 2 m.sec. and thus inertia effects must be accounted for in the calculation of the fracture moment.

The final part of this section is concerned with the effects of specimen geometry and impact velocity on the shape of the force-time response and values of the tear energies. The main purpose of these calculations is to illustrate the utility of the analysis. No experimental verification of the results has been carried out to date.

The material selected for this investigation is J-22 steel. A K_{Ic} of 100 ksi$\sqrt{\text{in}}$ is assumed on the basis of the experimental results discussed earlier. The crack speed is assumed to be ~3000 ft/sec. Four series of calculations have been performed to determine the effects of initial

impact velocity, specimen thickness, specimen length, and specimen notch depth to width ratio on the tear energies. The necessary data is shown in Table I. The tests are assumed to take place in the double pendulum impact machine. The force-time responses are generated by first calculating the midspan bending moment as a function of time (equation (34)) to establish t_1. The value of t_1 thus established along with a crack speed of 3000 ft/sec is then used to calculate F(t) from equation (30).

We first consider Series A (velocity effect). Figures 16, 17 and 18 show the force-time responses obtained for four initial velocities (29.4 ft/sec, 20 ft/sec, 10 ft/sec, 5 ft/sec). The curves in Fig. 16 need little explanation as we have seen this type of behavior before for brittle materials. The only important point to note is that the height of the peak is directly proportional to the velocity while t_1 is inversely proportional to the velocity. Inertia effects still need to be taken into account in the calculation of the fracture moment when $(V_{01}-V_{02})_0$ = 20 ft/sec (see Fig. 9).

When the velocity is decreased to 10 ft/sec, the force time response is now double peaked as shown in Fig. 17. This, of course, occurs because the value of t_1 is now large enough so that the minimum in the force-time response at

130μsec can develop. When the velocity is further decreased to 5 ft/sec, we see that the magnitude of the first peak decreases while magnitude of the second peak remains relatively constant at 15,000 lbs. This is to be expected since $t_1 > 200\mu$sec and thus the fracture moment is directly proportional to the hammer force as shown in equation (35). If we were to decrease the impact velocity even further, the first peak would become negligible while the magnitude of the second peak would be constant. The force-time response would thus become roughly triangular in shape; the base of the triangle increasing directly as the reciprocal of the velocity.

The tear energies calculated from equation (21a) are tabulated in Table I. Note the rapid decrease in ΔE between $(V_{01}-V_{02})_0 = 29.4$ ft/sec and $(V_{01}-V_{02})_0 = 20$ ft/sec. For initial velocities less than 20 ft/sec, ΔE decreases very slowly, asymptotically approaching the static value (that value of ΔE which would be observed in a static 3 point bend test).

Unfortunately, this assyptotic value of ΔE cannot be calculated using the present analysis. This is because the assumption of a linear F-α relationship is unwarranted for low velocities where the deformations at the contact point are primarily elastic. The static value of ΔE can be

estimated by assuming a Hertzian contact law and solving (6) for the case where the maximum bending moment is just less than the fracture moment. Since (6) is now a non-linear integral equation, however, no attempt is made here to obtain numerical values.

Figure 19 shows the effects of specimen thickness on the force-time response. We note here that the amplitude of the force-time response is directly proportional to the thickness but the time dependence is unchanged. From equation (18), it is evident the bending moment is also proportional to the specimen thickness and from equation (25), we see that the same is true for the fracture moment. Therefore t_1 is independent of thickness and the tear energy (from (21a)) per unit area is constant. This is shown in Table I.

Figures 20 and 21 show the effects of specimen length and notch depth to width ratio on the force-time response. The tear energies are again shown in Table I. Here it is seen that ΔE increases significantly with specimen length but remains relatively independent of the notch depth (the result for $a/2h = 0.5$ should not be taken too literally since the approximation of $Y_i(\xi)$ and ω_i used here is likely to give misleading results for deep notches).

To close this section, we have shown that the tear energies per unit area for a brittle material change significantly with specimen length and initial impact velocity but are relatively independent of the notch depth to width ratio and the specimen thickness. An important point to keep in mind, however, is that the dynamic tear energy is really the sum of the fracture energy plus the residual kinetic energy in the broken specimen (rotational + translational + vibrational) plus the plastic energy dissipated at the impact point. Thus the results obtained here do not necessarily imply that the fracture energy per unit area behaves in the same manner. This is an area which needs to be studied further.

CONCLUSIONS AND SUGGESTIONS FOR FUTURE WORK

The analysis presented here predicts impact forces which are in good agreement with the experimentally determined values for the J-22 and L-14 steel specimens. For the ductile 6061 aluminum, the predicted forces agree reasonably well with the experimental values in the initial portion when gross specimen yielding is not an important factor. The theoretical prediction of the bending moment prior to crack initiation is quite good for the J-22 steel and the 6061 aluminum. The experimental data available for the L-14 steel does not yet allow us to make a comparison with the

theoretical midspan bending moments because of the brittle weld failure prior to fracture initiation in the specimen. The theoretical and experimental bending moments at quarter span, however, agree rather well.

There are two primary conclusions which may be drawn at this stage of the investigation. First, all available results to date indicate that inertial effects are quite important in the early stages of the tear test and must be taken into account when calculating the midspan bending moment (assumed proportional to K_I) and also when interpreting the force-time responses. Second, it appears that the tear energy is not constant with specimen length and initial impact velocity. This points out the need for standardization of the test conditions and specimen geometries in dynamic tear testing.

As was indicated earlier, much work remains to be done. Some suggested areas of future work are enumerated below:

1. Inclusion of the results derived in the last part of Appendix I in the computer program for the impact forces and bending moments.

2. Consideration of the effects of gross specimen yielding on the force-time and moment-time responses. This could be accomplished using the normal mode technique proposed by Salvadori and Bleich [9] and would require only a slight modification of the elastic analysis.

3. Careful evaluation of the residual kinetic energy of the specimen after fracture. This is especially important for brittle materials since this energy may be a major portion of the tear energy.

NOTE ADDED IN PROOF:

Upon completion of this manuscript, the results of Venzi, Priest, and May (BISRA Open Report, "Influence of Inertial Load in Instrumented Impact Tests") have been brought to the author's attention. They reach essentially the same conclusions as stated here, although they are primarily concerned with instrumented Charpy tests. In fact, Fig. 21 on page 28 of their report is remarkably similar to Figs. 9 and 15 of this report.

REFERENCES

1. Goldsmith, W., Impact, The Theory and Physical Behavior of Colliding Solids, Edward Arnold Ltd., London, (1960), pp. 108-120.
2. Gurtin, M. E., "Variational Principles for Linear Elastodynamics," Archive for Rational Mechanics and Analysis, Vol. 16, (1964), pp. 34-50.
3. Nash, G. E. and Lange, E. A., "Mechanical Aspects of the Dynamic Tear Test", to be published in the Journal of Basic Engineering.
4. Goldsmith, W., ibid, pp. 82-96.
5. Timoshenko, S. P., "Zur Frage Nach der Wirkung Eines Stosse Auf einer Balken," Zietschrift fur Mathematick und Physik, Vol. 62, (1913), p. 198.
6. Roberts, G. E. and Kaufman, H., Tables of Laplace Transforms, W. Sanders Co., Philadelphia, (1966), p. 197.
7. Paris, P. C. and Sih, G. C., "Stress Analysis of Cracks" in Fracture Toughness Testing and Its Applications, ASTM STP 381, (1964), pp. 58-59.
8. Gross, B. and Srawley, J. E., "Stress Intensity Factors for Three-Point Bend Specimen by Boundary Collocation," NASA TN D-3092, (1965).
9. Bleich, H. H. and Salvadori, M. G., "Impulsive Motion of Elasto-Plastic Beams," Trans. ASCE, Vol. 120, (1955), p.499.

10. Gurtin, M. E., ibid, pp. 36-40.

11. Gurtin, M. E., ibid, pp. 41-42.

12. Howe, C. E. and Howe, R. M., "Application of the Electronic Differential Analyzer to the Oscillation of Beams Including Shear and Rotary Inertia," J. of Applied Mechanics, Vol. 21 (1955), p. 13.

13. Huang, T. C., "The Effect of Rotary Inertia and Shear Deformation on the Frequency and Normal Mode Equations of Uniform Beams with Simple End Conditions," J. of Applied Mechanics, Vol. 28, (1961), p. 579.

14. Chen, Y., Vibrations; Theoretical Methods, Addison-Wesley Pub. Co., Reading, Mass., (1966) pp. 215-218.

15. Neuber, H., Theory of Notch Stresses, Edwards Pub. Co., Ann Arbor, Mich., (1946).

16. Popov, E. P. "Mechanics of Materials," Prentice-Hall, Inc., Englewood Cliffs, N. J., (1961), pp. 287-299.

17. De Jager, E. M., "Applications of Distributions in Mathematical Physics," Mathematical Centre Tracts, 1964.

18. Lovitt, W. V., Linear Integral Equations, Dover Publications, Inc., New York, (1950), Chap. II.

APPENDIX I

DERIVATION OF THE ONE DIMENSIONAL BEAM EQUATIONS AND AN APPROXIMATE SOLUTION

Theorem: Let K be the set of all admissible states that meet the strain-displacement equations. Let $S = [\underset{\sim}{u}, \underset{\sim}{\varepsilon}, \underset{\sim}{\tau}]$ and for each $t \in [0, \infty)$ define the following functional $\Theta_t\{S\}$ over K:

$$\Theta_t\{S\} = \int_R [t*\tau_{ij}*\varepsilon_{ij}]d\underset{\sim}{x} - \frac{1}{2}\int_R \kappa_{ijkl}[t*\tau_{ij}*\tau_{kl}]d\underset{\sim}{x} + \tag{I.1}$$

$$+ \frac{1}{2}\int_R \rho[u_i*u_i]d\underset{\sim}{x} - \int_R [f_i*u_i]d\underset{\sim}{x} - \int_{B_i} [t*T_i*(u_i-\hat{u}_i)]d\underset{\sim}{x} -$$

$$- \int_{B_2} [t*\hat{T}_i*u_i]d\underset{\sim}{x}$$

(summation convention)

Then $\delta\Theta_t = 0$ over K if and only if S is a solution to the mixed problem, i.e., all the field equations, boundary conditions, and initial conditions are satisfied.

The proof of this theorem may be found in Gurtin's paper [2]. An admissible state is defined as an ordered array of tensor valued functions $\underset{\sim}{u}$, $\underset{\sim}{\varepsilon}$, $\underset{\sim}{\tau}$; i.e. $S = [\underset{\sim}{u}, \underset{\sim}{\varepsilon}, \underset{\sim}{\tau}]$ such that certain continuity conditions on $R \times [0, \infty)$ and the symmetry relations $\tau_{ij} = \tau_{ji}$, $\varepsilon_{ij} = \varepsilon_{ji}$; are satisfied. The notation $[f*g]$ is a shorthand for the convolution of f and g:

$$[f*g] \equiv \int_0^t f(t-\tau)g(\tau)d\tau = \int_0^t g(t-\tau)f(\tau)d\tau \tag{I.2}$$

$\delta\Theta_t$ is used to denote the first variation of Θ_t which is defined as follows:

$$\delta\Theta_t\{S\} = \frac{d}{d\lambda}\,\Theta_t\,\{S + \lambda\bar{S}\}\Big|_{\lambda = 0} \tag{I.3}$$

for S, $\bar{S} \in K$ and every real λ.

Let us now consider a uniform rectangular beam loaded along the top ($y = -h$) with a load per unit length $p(x)$. Assume the stresses and displacements in the following form:

$$\underset{\sim}{\tau} = \begin{pmatrix} \tau_{xx} & \tau_{xy} & o \\ \tau_{xy} & o & o \\ o & o & o \end{pmatrix}, \quad \underset{\sim}{u} = \begin{pmatrix} u_x \\ u_y \\ o \end{pmatrix} \tag{I.4}$$

where

$$\begin{aligned} \tau_{xx} &= M(x,t)G(y) \\ \tau_{xy} &= V(x,t)P(y) \\ u_x &= u_x(x,y,t) \\ u_y &= u_y(x,y,t) \end{aligned} \tag{I.5}$$

and $G(y)$, $P(y)$ are presumed known. If M and V are to be identified as the bending moment and shear force respectively, the additional conditions:

$$\int_A\!\!\int yG(y)dA = \int_A\!\!\int P(y)dA = 1 \tag{I.6}$$

must also be imposed. Substituting (I.4) and (I.5) into (I.1) gives:

$$\Theta_t\{S\} = -\int_0^L [t*M*\frac{\partial\alpha}{\partial x}]dx - \int_0^L [t*V*\alpha]dx +$$

$$+ \int_0^L [t-V-\frac{\partial\beta}{\partial x}]dx - \frac{1}{2}\int_0^L \Phi_1(\frac{1}{E})[t*M*M]dx -$$

$$- \frac{1}{2}\int_0^L \Phi_2(\frac{1}{G})[t*V*V]dx + \frac{\rho}{2}\int_0^L \Phi_3[\alpha*\alpha]dx +$$

$$+ \frac{\rho}{2}\int_0^L \Phi_4[\beta*\beta]dx - \int_0^L \frac{u_y}{\beta}\Big|_{y=-h}[t*p*\beta]dx +$$

$$+ [t*M-(\alpha-\hat{\alpha})]_{x=0}^{x=L} - [t*V-(\beta-\hat{\beta})]_{x=0}^{x=L} -$$

$$- \int_0^L \rho\Phi_3[\{t*\dot{\alpha}(0,x) + \alpha(0,x)\}*\alpha]dx -$$

$$- \int_0^L \rho\Phi_4[\{t*\dot{\beta}(0,x) + \beta(0,x)\}*\beta]dx \tag{I.7}$$

where

$$\alpha \equiv \int_A\int G(y)u_x dA, \qquad \beta \equiv \int_A\int P(y)u_y dA \tag{I.8}$$

$$\Phi_1 \equiv \int_A\int G^2(y)dA, \quad \Phi_2 = \int_A\int P^2(y)dA, \quad \Phi_3 \equiv \int_A\int \left(\frac{u_x}{\alpha}\right)^2 dA,$$

$$\Phi_4 = \int_A\int \left(\frac{u_y}{\beta}\right)^2 dA$$

and $G = -\frac{dP}{dy}$

Also, it should be noted that u_x and u_y must be in the form:

$$u_x(x,y,t) = U_x(x,t)\ Q(x,y)$$

$$u_y(x,y,t) = U_y(x,t)\ R(x,y) \tag{I.9}$$

so that Φ_3 and Φ_4 are time independent.

Taking the first variation of $\Theta_t\{S\}$ gives with the aid of (I.3) and the elementary properties of convolutions.

$$\delta\Theta_t\{S\} = \int_0^L [\{- t*\frac{\partial\alpha}{\partial x} - \frac{\Phi_1}{E} t*M\}*\bar{M}]dx +$$

$$+ \int_0^L [\{-t*\alpha + t*\frac{\partial\beta}{\partial x} - \frac{\Phi_2}{G}t*V\}*\bar{V}]dx +$$

$$- \int_0^L [\{-t*\frac{\partial M}{\partial x} + t*V - \rho\Phi_3\alpha + \Phi_3 J_x\}*\bar{\alpha}]dx +$$

$$+ \int_0^L [\{- t*\frac{\partial V}{\partial x} + \rho\Phi_4\beta - \frac{U_y}{\beta}\Big|_{y=-h}(t*P) - \Phi_4 J_y\}*\bar{\beta}]dx +$$

$$+ [t*(\alpha-\hat{\alpha})*\bar{M}]\Big|_{x=0}^{x=L} - [t*(\beta-\hat{\beta})*\bar{V}]\Big|_{x=0}^{x=L} \qquad \text{(I.10)}$$

where

$$J_x \equiv \rho[t\dot{\alpha}(0,x) + \alpha(0,x)]$$

$$J_y \equiv \rho[t\dot{\beta}(0,x) + \beta(0,x)] \qquad \text{(I.11)}$$

Setting $\delta\Theta_t = 0$, we have with the aid of Gurtin [10]:

1) $-t*\frac{\partial\alpha}{\partial x} - \frac{\Phi_1}{E}t*M = 0$

2) $-t*\alpha + t*\frac{\partial\beta}{\partial x} - \frac{\Phi_2}{G}t*V = 0$

3) $-t*\frac{\partial M}{\partial x} + t*V - \rho\Phi_3\alpha + \Phi_3 J_x = 0$

(I.12)

4) $$- t^* \frac{\partial V}{\partial x} + \rho \Phi_4 \beta - \frac{u_y}{\beta}\Big|_{y=-h} (t^* p) - \Phi_4 J_y = 0$$

5) $\alpha = \hat{\alpha}$ or $\bar{M} = 0$ and $\beta = \hat{\beta}$ or $\bar{V} = 0$ on $x = 0$, $x = L$

From Gurtin [11], it can be shown that when equations 3 and 4 of (I.12) are satisfied, the following equations along with the intial conditions on $\dot{\alpha}(0,x)$, $\alpha(0,x)$, $\dot{\beta}(0,x)$, $\beta(0,x)$ are also satisfied:

1) $$\frac{\partial M}{\partial x} - V + \rho \Phi_3 \frac{\partial^2 \alpha}{\partial t^2} = 0$$

2) $$\frac{\partial V}{\partial x} - \rho \Phi_4 \frac{\partial^2 \beta}{\partial t^2} + \frac{u_y}{\beta}\Big|_{y=-h} p = 0 \qquad \text{(I.13)}$$

Equations (I.13) are the generalized equilibrium equations Differentiating 1. and 2. of (I.12) twice with respect to time gives the generalized stress-displacement equations.

1) $$M = - \frac{E}{\Phi_1} \frac{\partial \alpha}{\partial x}$$

2) $$V = \varkappa \left(\frac{\partial \beta}{\partial x} - \alpha\right) \qquad \text{where } \varkappa \equiv G/\Phi_2 \qquad \text{(I.14)}$$

Finally, equations 5. of (I.12) are the boundary conditions. Either α or M and either β or V must be specified at x=0, x=L.

If we take the stresses and displacements as:

$$u_x = - U_x y$$

$$u_y = u_y(x,t)$$

$$\tau_{xx} = \frac{My}{I}$$

$$\tau_{xy} = \frac{V}{2I}(h^2 - y^2) \qquad \text{(I.15)}$$

then:

$$\alpha = + U_x(x,t) \qquad \Phi_3 = I$$

$$\beta = u_y(x,t) \qquad \varkappa = 5/6\ GA$$

$$\Phi_1 = 1/I$$

$$\Phi_4 = A$$

the field equations now become:

$$1)\quad \frac{\partial M}{\partial x} - V + \rho\Phi_3 \frac{\partial^2 d}{\partial t^2} = 0$$

$$2)\quad \frac{\partial V}{\partial x} - \rho A \frac{\partial^2 u_y}{\partial t^2} + p = 0$$

$$3)\quad M = - EI \frac{\partial U_x}{\partial x}$$

$$4)\quad V = \varkappa \left(\frac{\partial u_y}{\partial x} - U_x\right) \tag{I.17}$$

which are the well known field equations for a Timoshenko beam.

Now consider the notched beam shown in Fig. 2. Let us assume that the normal and shear stress distributions can be approximated in the following manner:

$$\tau_{xx} = M(x,t)G_1(y) \qquad x \in [0, \tfrac{L-\delta}{2}]$$

$$\tau_{xy} = V(x,t)P_1(y)$$

$$\tau_{xx} = M(x,t)\ G_2(y) \qquad x \in [\tfrac{L-\delta}{2}, \tfrac{L+\delta}{2}]$$

$$\tau_{xy} = V(x,t)\ P_2(y)$$

$$\tau_{xx} = M(x,t)\ G_3(y) \qquad x \in [\tfrac{L+\delta}{2}, L]$$

$$\tau_{xy} = V(x,t)\ P_3(y) \tag{I.18}$$

If τ_{yy} is ignored as well as the discontinuity in cross sectional area due to the notch, than (I.13) and (I.14) can be applied in each of the three regions:

$$
\begin{aligned}
&1)\quad \frac{\partial M}{\partial x} - V + \rho\Phi_{3i}\frac{\partial^2\alpha}{\partial t^2} = 0 \\
&2)\quad \frac{\partial V}{\partial x} - \rho\Phi_{4i}\frac{\partial^2\beta}{\partial t^2} + \frac{u_y}{\beta}\Big|_{y=-h} p = 0 \\
&3)\quad M = -\frac{E}{\Phi_{1i}}\frac{\partial\alpha}{\partial x} \qquad\qquad x\in[x_{i-1},x_i] \\
&4)\quad V = \varkappa_i\left(\frac{\partial\beta}{\partial x} - \alpha\right) \qquad\qquad i = 1,2,3
\end{aligned}
\tag{I.19}
$$

where

$$
\begin{aligned}
&\Phi_{1i} \equiv \int_A\!\!\int G_i^{\,2}(y)dA, \quad \Phi_{2i} \equiv \int_A\!\!\int P_i^{\,2}(y)dA \\
&\Phi_{3i} \equiv \int_A\!\!\int \frac{u_x}{\alpha}^{2} dA, \quad \Phi_{4i} \equiv \int_A\!\!\int \frac{u_y}{\beta}^{2} dA
\end{aligned}
\tag{I.20}
$$

$$
\left.\begin{aligned} G_i &= G \\ P_i &= P \end{aligned}\right\} \quad x\in[x_{i-1},\ X_i]
$$

and $x_0 = 0$, $x_1 = \frac{L-\delta}{2}$, $x_2 = \frac{L+\delta}{2}$, $x_3 = L$

Of course, the solutions in each region must satisfy continuity conditions on M, V, α, β at the interior points x_i.

We now consider the solutions to equations (I.19). In general, Φ_{3i} and Φ_{4i} are not constant in the interval $[x_{i-1}, x_i]$ but are functions of x. We can solve (I.19) using normal mode theory, but to find the normal modes, requires one to solve four ordinary differential equations with variable coefficients. Although this is possible with the aid of an analog computer (see for example Howe and Howe

[12]), this technique will not be discussed further in this paper.

If the displacements u_x and u_y can be expressed as:

$$\begin{aligned} u_x &= U_x(x,t)Q_i(y) \\ u_y &= U_y(x,t)R_i(y) \end{aligned} \qquad (i = 1,2,3) \tag{I.21}$$

then Φ_{3i} and Φ_{4i} are constant in the interval $[x_{i=1}, x_i]$. The situation now becomes somewhat more simplified and we can use normal mode theory to solve (I.19) where the normal modes can be obtained using the solution due to Huang [13]. The computational difficulties are still formidible, however, primarily due to the two modes of wave transmission permitted in a Timoshenko type beam.

In view of the assumption involving the normal stress τ_{yy} and the requirement $G(y) = \frac{dP}{dy}$, it is the author's opinion that the effort required to obtain the solution to (I.19) is not justified. Therefore, the following additional assumptions will be made. First, assume that the effects of rotary inertia can be ignored. This implies $\Phi_3 = 0$ which in turn implies:

$$\frac{\partial M}{\partial x} = V \tag{I.22}$$

Next, assume that the shear deflection is negligible. This implies:

$$\alpha = \frac{\partial \beta}{\partial x} \tag{I.23}$$

and also, since the shear force V is generally nonzero, $\varkappa \to \infty$.

Substituting (I.22) and (I.23) into (I.19) gives:

$$\frac{E}{\Phi_{1i}} \frac{\partial^4 \beta}{\partial x^4} + \rho \Phi_{4i} \frac{\partial^2 \beta}{\partial t^2} = \left(\frac{u_y}{\beta}\right) p_{y=-h} \tag{I.24}$$

for $x \in [x_{i-1}, x_i]$

Making a final assumption on u_y:

$$u_y(x,y,t) = u_y(x,t) \tag{I.25}$$

gives:

$$\frac{E}{\Phi_{1i}} \frac{\partial^4 u_y}{\partial x^4} + \rho A_g \frac{\partial^2 u_y}{\partial t^2} = p \tag{I.26}$$

The effect of the notch is thus reflected solely in the term Φ_{1i}. The validity of all these assumptions can only be verified by comparison with experimental results although it is known for uniform beams that when the duration of impact is on the order of the fundamental period, (as in our case) the effects of shear and rotary inertia can be neglected.

We will now consider the solution to (I.26). Let $\xi = \frac{x}{L}$, then (I.26) becomes:

$$\frac{E}{L^4 \Phi_{1i}} \frac{\partial^4 u_y}{\partial \xi^4} + \rho A_g \frac{\partial^2 u_y}{\partial t^2} = p(\xi,t) \tag{I.27}$$

Assume that $u_y(\xi,t)$ for the homogeneous version of (I.27) can be expressed as:

$$u_{yi}(\xi,t) = Y_i(\xi) e^{j\omega t} \tag{I.28}$$

where

$u_{yi}(\xi,t) = u_y(\xi,t)$ for $\xi \epsilon [\xi_{i-1}, \xi_1]$ (i=1,2,3) and $j \equiv \sqrt{-1}$. Substituting (I.28) into (I.27) and solving the resulting ordinary differential equation gives:

$$Y_i(\xi) = C_{1i} \cosh N_i k\xi + C_{2i} \sinh N_i k\xi + \\ + C_{3i} \cos N_i k\xi + C_{4i} \sin N_i k\xi \tag{I.29}$$

where

$$k \equiv \frac{\rho A L^4 \omega^2}{EI_g} \quad \text{and} \quad N_i \equiv I_g \, \Phi_{1i}$$

The twelve constants in (I.29) as well as the frequency ω can be found by applying the boundary conditions at $\xi = 0$, $\xi = 1$ as well as the continuity conditions on M, V, u_y and $\partial u_y/\partial \xi$ at ξ_1 and ξ_2. This procedure yields a countably infinite set of eigenvectors $Y_m(\xi)$ (m = 1,2,...) and eigenvalues ω_m. The eigenvector $Y_m(\xi)$ for $\xi \epsilon [0,1]$ is defined as:

$$Y_m(\xi) = \sum_{i=1}^{3} Y_{mi}(\xi)[H(\xi-\xi_{i-1}) - H(\xi-\xi_i)] \tag{I.30}$$

where H denotes the Heaviside unit step function.

Once the eigenvalues and eigenvectors are known, the solution of the non homogeneous equation (I.27) follows directly. Assume $u_{yi}(\xi,t)$ in the form (we follow Chen [14] here):

$$u_{yi}(\xi,t) = \sum_{m=1}^{\infty} Y_{im}(\xi) T_m(t) \tag{I.31}$$

Substituting (I.31) into (I.27), it is easily shown that:

$$T_m(t) = \frac{1}{\omega_m}\int_0^t R_m(\tau)\sin\omega_m(t-\tau)d\tau + A_m\sin\omega_m t + B_m\cos\omega_m t \tag{I.32}$$

where $R_m(t)$ is unknown at this point. $R_m(t)$ can be found, however, using the orthogonality condition:

$$\rho A_g\int_0^1 Y_m(\xi)Y_m(\xi)d\xi = 0 \qquad (m \neq n) \tag{I.33}$$

Thus, $R_m(t)$ is given by:

$$R_m(t) = \frac{1}{W_m}\int_0^1 p(\xi,t)Y_m(\xi)d\xi \tag{I.34}$$

where

$$W_m = \int_0^1 \rho A_g Y_m^2(\xi)d\xi$$

For a concentrated load at midspan,

$$p(\xi,t) = F(t)\ \delta(\xi-1/2) \tag{I.35}$$

and from (I.31), (I.34), and (I.32), we have;

$$u_y(\xi,t) = \sum_{m=1}^{\infty}(A_m\sin\omega_m t + B_m\cos\omega_m t)Y_m(\xi) + \tag{I.36}$$

$$+ \sum_{m=1}^{\infty}\frac{Y_m(\xi)Y_m(1/2)}{\omega_m W_m}\int_0^t F(\eta)\sin\omega_m(t-\eta)d\eta$$

The bending moment $M(\xi,t)$ can now be found easily. From (I.19) (equation 3.) and (I.23) we have:

$$\frac{-E}{L^2\Phi_{1i}}\ \frac{\partial^2 u_y}{\partial\xi^2} = M(\xi,t) \tag{I.37}$$

The problem of determining the bending deflections and moments for the notched beam is now solved once Φ_{1i} and δ are known as a function of the beam geometry. To estimate them, we now assume that τ_{xx} can be approximated as follows:

$$\tau_{xx} = \frac{My}{I_g} \qquad x \in [0, \tfrac{L-\delta}{2}] \text{ and } x \in [\tfrac{L+\delta}{2}, L]$$

$$\tau_{xx} = C_1 \left[\frac{(h-y)}{\{(h-y)^2 - a^2\}^{1/2}} - 1 \right] + C_2 y \tag{I.37}$$

for $-h \leq y \leq h-a-\Delta$

$$\tau_{xx} = \sigma_n K_t = \left[\frac{6M}{b(2h)^2(1-a/2h)^2} \right] K_t \qquad x \in [\tfrac{L+\delta}{2}, \tfrac{L-\delta}{2}]$$

for $h-a-\Delta \leq y \leq h-a$

$$\tau_{xx} = 0$$

for $h-a \leq y \leq h$

C_1 and C_2 are as yet undetermined functions of $(a/2h)$ but must be linear functions of M. K_t is the elastic stress concentration factor and depends on (a/R); Δ is an as yet undetermined length depending on (a/R) and $(a/2h)$. Equation (I.37) should provide a reasonable approximation for relatively short, sharp notches.

To determine C_1 and C_2, we use the two available equilibrium conditions at the beam cross section:

$$1. \quad b\int_{-h}^{h-a} \tau_{xx} dy = 0 \qquad\qquad 2. \quad b\int_{-h}^{h-a} y\tau_{xx} dy = M \tag{I.38}$$

Assuming $(\Delta/a) <<< 1$, it is easily shown that

$$\tau_{xx} = \frac{M}{\Lambda b(2h)^2}\left[\frac{(h-y)}{\{(h-y)^2-a^2\}^{1/2}} - 1 + \frac{y}{2h}\,\Omega\right] \tag{I.39}$$

where Λ, Ω are functions of a/2h alone and are given by the following expressions:

$$\Lambda = \frac{(a/2h)^2}{2}\ln\left\{\frac{a/2h}{1+[1-(a/2h)^2]^{1/2}}\right\} + \frac{a/2h}{2}(1-a/2h) + \frac{\Omega}{3}\left\{\left(\frac{1}{2}-a/2h\right)^3 + \frac{1}{8}\right\} \tag{I.40}$$

$$\Omega = \frac{2}{a/2h}\left\{\frac{[1-(a/2h)^2]^{1/2}}{(1-a/2h)} - 1\right\}$$

Using the definition of Φ_{1i} (equation (I.20), we can now find Φ_{11}, Φ_{12}, Φ_{13}.

When $(\Delta/a) <<< 1$, Φ_{12} is easily shown to be given by:

$$\Phi_{12} = \frac{1}{12\Lambda^2 I_g}\left\{\frac{\Omega}{3}\left[(1/2-a/2h)^3 + 1/8\right] + (a/2h)^2\ln\left[\frac{a/2h}{1+[1-(a/2h)^2]^{1/2}}\right] + a/2h\left[\mathrm{ctnh}^{-1}(1+\Delta/a) - \mathrm{ctnh}^{-1}\left(\frac{1}{a/2h}\right) + 1/2\right]\right\}$$

Also,

$$\Phi_{11} = \Phi_{13} = 1/I_g \tag{I.42}$$

(Δ/a) may be found as follows: From equation (I.39),

$$\tau_{xx}\Big|_{y=h-a-\Delta} \cong \frac{M}{\Lambda b(2h)^2}\left\{\frac{a/2h}{2\Delta/2h}\right\}^{1/2} \tag{I.43}$$

But from equation (I.37),

$$\tau_{xx}\Big|_{y=h-a-\Delta} = \frac{6M}{b(2h)^2(1-a/2h)^2} K_t \tag{I.44}$$

therefore,

$$K_t = \frac{(1-a/2h)^2}{6\Lambda} \left\{\frac{a/2h}{2\Delta/2h}\right\}^{1/2} \tag{I.45}$$

But K_t is also given by [15]:

$$K_t = 2(a/R)^{1/2} \tag{I.46}$$

and therefore, setting (I.46) equal to (I.45), we have:

$$\Delta/a = \frac{(1-a/2h)^4}{36\Lambda^2} \left(\frac{R/a}{8}\right) \tag{I.47}$$

Table II shows Δ/a and Φ_{12} for three values of a/2h (.1, .2, .3) with $R/a = 10^{-2}$.

To estimate δ, we consider now the static deflections of a simply supported notched beam loaded at midspan with a concentrated force F. Thus we must solve the time independent version of equation (I.27):

$$\frac{E}{\Phi_{1i}} \frac{d^4u_y}{dx^4} = F\,\delta(x-L/2) \qquad x \in [x_{i-1}, x_i] \quad i = 1,2,3 \tag{I.48}$$

The deflection at midspan, $u_y(L/2)$, is easily obtained by the moment-area method [16]. Thus we have:

$$u_y(L/2) = \frac{FL^3}{48EI_g}(1-\delta/L)^3 \left[1+3N_2 \frac{\delta/L}{1-\delta/L} + 3N_2\left(\frac{\delta/L}{1-\delta/L}\right)^2 + \frac{5N_2}{4}\left(\frac{\delta/L}{1-\delta/L}\right)^3\right] \tag{I.49}$$

where $N_2 = I_g\,\Phi_{12}$

However, the deflection at midspan is also given by (27) as:

$$u_y(L/2) = \frac{FL^3}{48EI_g}\left[1+\frac{h}{L}\Phi\right] \tag{I.50}$$

where $\Phi = 65(a/2h)^2 - 87.3(a/2h)^3 + 205(a/2h)^4$

Hence, comparing equations (I.49) and (I.50), we see that:

$$\left(1 - \frac{\delta}{L}\right)^3 \left[1+3N\left(\frac{\delta/L}{1-\delta/L}\right) + 3N\left(\frac{\delta/L}{1-\delta/L}\right)^2 + \frac{5N}{4}\left(\frac{\delta/L}{1-\delta/L}\right)^3\right] = 1+\frac{h}{L}\Phi \tag{I.51}$$

Once h/L is specified, equation (I.51) can be solved for δ/L as a function of (a/2h). Table II shows (δ/L) for three values of (a/2h) (.1, .2, .3) with (h/L) = 1/8.

As was stated previously, where δ and Φ_{1i} are known as functions of (a/2h), equation (I.27) may be solved to obtain the deflection u_y. This approach has some serious limitations, however. First is the complexity of the calculation, second is that the approximation for τ_{xx} is only good for shallow notches, i.e. (a/2h)<.3. Thus it is desirable to have an approximate solution of (I.27) which does not explicitly depend on the assumed form of τ_{xx}.

If we examine Table II, we note that (δ/L) is very small for all values of (a/2h) considered. This suggests that we form an approximate solution by letting $(\delta/L) \Rightarrow 0$. However, in order for the effect of the notch to be felt, $(\delta/L) \Rightarrow 0$ implies $\Phi_{12} \Rightarrow \infty$. We therefore approximate the actual beam

by a beam with Φ_1 (x) given by:

$$\Phi_1(x) = \frac{1}{I_g} + D\delta(x-L/2) \tag{I.52}$$

where D = D(a/2h). The coefficient D is determined by the condition that:

$$u_y(L/2)\Big|_{static} = \frac{FL^3}{48EI_g}\left(1+\frac{h}{L}\Phi\right) \tag{I.53}$$

For a beam with a variable Φ_1, the deflection equation (I.27) may be written as:

$$\frac{\partial^2}{\partial x^2}\left(\frac{E}{\Phi_1}\frac{\partial^2 u_y}{\partial x^2}\right) + \rho A_g \frac{\partial^2 u_y}{\partial t^2} = p = F\delta(x-L/2) \tag{I.54}$$

To find the static deflections, u_y, we set the time dependent term in (I.54) equal to zero and substitute (I.52) to get:

$$\frac{\partial^2}{\partial x^2}\left(\frac{E}{1/I_g+D\delta(x-L/2)}\right)\frac{\partial^2 u_y}{\partial x^2} = F\delta(x-L/2) \tag{I.55}$$

The solution of (I.55) for a simply supported beam may now be found easily by Laplace transform techniques. (Of course, (I.55) cannot be satisfied in the conventional sense at x = L/2; however, we assume that (I.55) is satisfied in the conventional sense at all other values of x and is satisfied from a distribution theory point of view at x = L/2. For a detailed discussion see [17].

Taking the Laplace transform of (I.55) twice, employing the boundary conditions:

$$u_y(0) = \frac{d^2u_y}{dx^2}\Big|_{x=0} = 0 \tag{I.56}$$

and inverting gives:

$$u_y = x\frac{du_y}{dx}\Big|_{x=0} + \left\{\frac{x^3}{6} + \frac{DLI_g}{2}(x-L/2)H(x-L/2)\right\}\frac{d^3u_y}{dx^3}\Big|_{x=0} + \\ + \frac{F}{6EI_g}(x-L/2)^2H(x-L/2) \tag{I.57}$$

The terms $\frac{du_y}{dx}\Big|_{x=0}$ and $\frac{d^3u_y}{dx^3}\Big|_{x=0}$ may be eliminated by using the remaining boundary conditions:

$$u_y(L) = \frac{d^2u_y}{dx^2}\Big|_{x=L} = 0 \tag{I.58}$$

After the necessary calculations are performed, we get:

$$u_y = x\left(\frac{3FL^2}{48EI_g} + \frac{PLD}{8E}\right) - \left\{\frac{x^3}{6} + \frac{DLI_g}{2}(x-L/2)H(x-L/2)\right\}\frac{F}{2EI_g} + \\ + \frac{F}{6EI_g}(x-L/2)^3H(x-L/2) \tag{I.59}$$

Finally, setting $x = L/2$ gives:

$$u_y(L/2) = \frac{FL^3}{48EI_g}\left(1 + \frac{3DI_g}{L}\right) \tag{I.60}$$

Equating (I.53) and (I.60) gives the following expression for D:

$$\frac{DI_g}{L} = \frac{1}{3}(h/L)\Phi \tag{I.61}$$

and moments.

Let us first consider the homogeneous version of (I.54):

$$\frac{\partial^2}{\partial x^2}\left(\frac{E}{1/I_g + D\delta(x-L/2)}\frac{\partial^2 u_y}{\partial x^2}\right) + \rho A_g \frac{\partial^2 u_y}{\partial t^2} = 0 \tag{I.62}$$

Assume:

$$u_y = Y(x)\ \sin\omega t \tag{I.63}$$

and substitute (I.63) into (I.62) to get:

$$\frac{d^2}{dx^2}\left(\frac{E}{1/I_g + D\delta(x-L/2)}\frac{d^2}{dx^2}\right) - \omega^2 AY = 0 \tag{I.64}$$

Taking the Laplace transform twice, employing the boundary conditions (I.56), and inverting gives:

$$\begin{aligned} Y = {} & \left.\frac{d}{dx}\right|_{x=0} (\sin kx + \sinh kx)\ (1/2k) + \\ & + \left.\frac{d^3Y}{dx^3}\right|_{x=0} (\sinh kx - \sin kx)\ (1/2k^3) + \frac{DI_g}{2k}\left(\frac{L}{2}\left.\frac{d^3Y}{dx^3}\right|_{x=0} + \right. \\ & \left. + k^4\epsilon\right) H(x-L/4)\ [\sin k(x-L/2) + \sinh\ k(x-L/2)] \end{aligned} \tag{I.65}$$

where

$$\epsilon = \int_0^{L/2} d\eta \int_0^{\eta} Y(\xi)\, d\xi \tag{I.66}$$

$$k^4 = \frac{\omega^2 A_g}{EI_g}$$

As in the analysis of the static deflections, the terms $\frac{dY}{dx}\Big|_{x=0}$ and $\frac{d^3Y}{dx^3}\Big|_{x=0}$ may be eliminated using the boundary conditions (I.58). The procedure yields:

$$Y(x) = 2Dk^2 I_g \epsilon \left[\frac{\sin kL \sinh\frac{kL}{2} \sinh kx + \sin\frac{kL}{2} \sinh kL \sin kx}{DIgkL\left(\sin\frac{kL}{2}\sinh kL - \sinh\frac{kL}{2}\sin kL\right) - \frac{4}{k}\sin kL \sinh kL} \right]$$

for $x \in [0, L/2)$ (I.67)

Integrating equation (I.67) twice from $x = 0$ to $x = L/2$ gives, using the definition of ϵ (equation (I.66)):

$$0 = \epsilon \left\{ 1 - \left[\frac{\left(\cosh\frac{kL}{2} - \cos\frac{kL}{2}\right) + \frac{2}{kL}\left(-\cosh\frac{kL}{2}\sin\frac{kL}{2}\right) + \cos\frac{kL}{2}\sinh\frac{kL}{2}}{\left(\cosh\frac{kL}{2} - \cos\frac{kL}{2}\right) - \frac{8}{DI_g Lk^2}\cosh\frac{kL}{2}\cos\frac{kL}{2}} \right] \right\}$$

(I.68)

But $\epsilon = 0$ corresponds to all the antisymmetric modes, therefore we must have:

$$1 - \left[\frac{\left(\cosh\frac{kL}{2} - \cos\frac{kL}{2}\right) + \frac{2}{kL}\left(-\cosh\frac{kL}{2}\sin\frac{kL}{2} + \cos\frac{kL}{2}\sinh\frac{kL}{2}\right)}{\left(\cosh\frac{kL}{2} - \cos\frac{kL}{2}\right) - \frac{8}{DI_g Lk^2}\cosh\frac{kL}{2}\cos\frac{kL}{2}} \right] = 0$$

(I.69)

for all symmetric modes. Equation (I.69) is thus the eigenvalue equation for the symmetric modes and reduces to:

$$\tan\frac{kL}{2} = \frac{2L}{DI_g\frac{kL}{2}} + \tanh\frac{kL}{2} \qquad \text{(I.70)}$$

Substituting equation (I.61), we have:

$$\tan\frac{kL}{2} = \frac{6}{(h/L)\Psi(\frac{kL}{2})} + \tanh\frac{kL}{2} \qquad \text{(I.71)}$$

Examining equation (I.71), we first note that for a uniform beam, $\Phi = 0$ which implies $\tan\frac{kL}{2} = \infty$. Thus $kL = n\pi (n = 1,3,5...)$ which are the eigenvalues for the symmetric modes of a uniform simply supported, Euler-Bernoulli beam. Going back to equation (I.67) and letting $kL = n\pi (n = 1,3,5...)$, we have:

$$Y(x)\Big|_{kL = n\pi} = \frac{2k\epsilon}{L} \sin kx \tag{I.72}$$

Equation (I.72) states that Y(x), for $kL = n\pi$, is proportional to sin kx which is again equivalent to the result obtained for the Euler-Bernoulli beam.

We now consider solutions to (I.71) for the case where $\Phi \neq 0$. Since Φ is a monotonically increasing function of (a/2h), we see that $kL<n\pi$ for all (a/2h) and decreases with increasing (a/2h). This of course implies that the natural frequencies ω_n decrease with increasing crack length. The first root of (I.72) (corresponding to the fundamental frequency) is shown in Table II for five values of (a/2h) (.1, .2, .3, .4, .5).

With the eigenvalues and eigenvectors now determined, equations (I.36) and (I.37) can now be used to supply the dynamic displacements and bending moments.

APPENDIX II

ITERATION TECHNIQUE FOR DETERMINATION OF THE HAMMER FORCE WITH HIGHER BENDING MODES ACCOUNTED FOR

For simplicity, cracking of the specimen will be neglected. t_k $(k = 1,2,\ldots) \to \infty$ and $F(t) = F_0(t)$ for $t \in [0, \infty)$. Thus the following integral equation must be considered:

$$\frac{F}{k_4} = (V_{01}-V_{02})t = k_1 \int_0^t F(\eta)(t-\eta)d\eta - \sum_{i=1}^{\infty} \frac{k_{3i}}{\omega_i} \int_0^t F(\eta)\sin\omega_i(t-\eta)d\eta \tag{II.1}$$

where

$$k_{3i} = \frac{Y_i^{\,2}(1/2)}{W_i}$$

To solve (II.1), we employ a successive approximation technique. Let F^0 be the initial approximation where $F^0(t)$ is given by:

$$F^0(t) = \frac{(V_{01}-V_{02})k_4}{\alpha\beta(\alpha^2-\beta^2)} \left[\alpha(\omega_1^{\,2}-\beta^2)\sin\beta t + \beta(\alpha^2-\omega_1^{\,2})\sin\alpha t\right] \tag{II.2}$$

and is the solution to (II.1) with a single non zero bending mode. Using $F^0(t)$, we calculate the elastic beam deflection $u_y^{\,0}(1/2, t)$ where

$$u_y^{\,0}(1/2, t) = \sum_{i=1}^{\infty} \frac{k_{3i}}{\omega_i} \int_0^t F^0(\eta)\sin\omega_i(t-\eta)d\eta \tag{II.3}$$

obtained from the equation:

$$\frac{F^1}{k_4} = (V_{01}-V_{02})\ t - k_1 \int_0^t F^1(\eta)(t-\eta)d\eta - u_y{}^0(1/2,\ t) \tag{II.4}$$

Let $F^1 \equiv F^0 + \Delta F^{1,0}$, then we have from (II.1), (II.3), and (II.4):

$$\frac{\Delta F^{1,0}}{k_4} = -\ k_1 \int_0^t \Delta F^{1,0}(\eta)(t-\eta)d\eta - \sum_{i=2,3,\ldots}^{\infty} \frac{k_{3i}}{\omega_i} \int_0^t F^0(\eta) \times$$

$$\times \quad \sin\omega_i(t-\eta)d\eta \tag{II.5}$$

Taking the Laplace transform of (II.5), we have:

$$\frac{\Delta\bar{F}^{1,0}}{k_4} = \sum_{i=2}^{\infty} k_{3i}\ \bar{F}^0 \left(\frac{p^2}{(p^2+\omega_i{}^2)(p^2+k_1k4)}\right) \tag{II.6}$$

Equation (II.6) is easily inverted to give:

$$\Delta F^{1,0} = k_4 \sum_{i=2,3}^{\infty} k_{3i} \int_0^t F^0(\eta)\ \frac{1}{(\omega_i{}^2-k_1k_4)}\ [\omega_i \sin\omega_i(t-\eta)\ -$$

$$-\ \sqrt{k_1k_4}\ \sin\sqrt{k_1k_4}\ (t-\eta)]d\eta \tag{II.7}$$

Let $F^2(t)$ be the next approximation where $F^2(t)$ is obtained from:

$$\frac{F^2}{k_4} = (V_{01}-V_{02})t - k_1 \int_0^t F^2(\eta)(t-\eta)d\eta - u_y{}^1(1/2,t) \tag{II.8}$$

and

$$u_y{}^1(1/2,t) = \sum_{i=1}^{\infty} \frac{k_{3i}}{\omega_i} \int_0^t F^1(\eta)\sin\omega_i(t-\eta)d\eta \tag{II.9}$$

Setting $F^2 = F^1 + \Delta F^{2,1}$, we have from (II.4) and (II.8):

$$\frac{\Delta F^{2,1}}{k_4} = - k_1\int_0^t \Delta F^{2,1}(\eta)(t-\eta)d\eta - \sum_{i=1}^{\infty} \frac{k_{3i}}{\omega_i} \int_0^t \Delta F^{1,0}(\eta)\sin\omega_i(t-\eta)d\eta \tag{II.10}$$

Solving (II.9) for $\Delta F^{2,1}$ by Laplace transforms again, we get:

$$\frac{\Delta F^{2,1}}{k_4} = - \sum_{i=1}^{\infty} k_{3i}\int_0^t \Delta F^{1,0}(\eta) \frac{1}{(\omega_i^2-k_1k_4)} [\omega_i\sin\omega_i(t-\eta) - \\ - \sqrt{k_1k_4} \sin \sqrt{k_1k_4}(t-\eta)]d\eta \tag{II.11}$$

If we continue this procedure, we have in general:

$$\frac{F^n}{k_4} = (V_{01}-V_{02})t-k_1\int_0^t F^n(\eta)(t-\eta)d\eta - u_y^{n-1}(1/2,t) \tag{II.12}$$

where

$$u_y^{n-1}(1/2,t) = \sum_{i=1}^{\infty} \frac{K_{3i}}{\omega_i} \int_0^t F^{n-1}(\eta)\sin\omega_i(t-\eta)d\eta \tag{II.13}$$

and

$$\Delta F^{n+1,n} = - k_4 \sum_{i=1}^{\infty} k_{3i}\int_0^t \Delta F^{n,n-1}(\eta) \frac{1}{(\omega_i^2-k_1k_4)}[\omega_i\sin\omega_i(t-\eta) - \\ - \sqrt{k_1k_4} \sin \sqrt{k_1k_4}(t-\eta)]d\eta \tag{II.14}$$

for n = 1,2.....

The convergence of this procedure can be established very easily by employing the argument presented in Lovitt [18]. The details will not be shown here due to length considerations.

TABLE I

$(V_{01}-V_{02})$ ft/sec	L in	2h in	a/2h	b in	α $in^{5/2}$	$\Delta E/A$ net $\frac{ft\text{-}lb}{in^2}$
Series A (Velocity Effect) J-22						
29.4	6.5	1.625	0.307	0.625	0.202	78.5
20.0	6.5	1.625	0.307	0.625	0.202	39.2
10.0	6.5	1.625	0.307	0.625	0.202	34.2
5.0	6.5	1.625	0.307	0.625	0.202	30.6
Series B (Thickness Effect) J-22						
29.4	6.5	1.625	0.307	0.625	0.202	78.5
29.4	6.5	1.625	0.307	1.25	0.404	78.5
29.4	6.5	1.625	0.307	1.75	0.580	78.5
Series C (Length Effect) J-22						
29.4	7	1.625	0.307	0.625	0.202	83.0
29.4	9	1.625	0.307	0.625	0.202	104
29.4	11	1.625	0.307	0.625	0.202	122
Series D (Notch Depth Effect) J-22						
29.4	6.5	1.625	0.10	0.625	0.373	69.6
29.4	6.5	1.625	0.30	0.625	0.202	78.0
29.4	6.5	1.625	0.50	0.625	0.120	104

$$M = K_I \sqrt{\frac{(2h)^3 b^2}{\chi^2}} \equiv K_I \alpha$$

TABLE II

$a/2h$	Δ/a	$I_g\Phi_{12}$	δ/L	$kL^{(1)}$	ω_1/ω_1^0
.1	8.4×10^{-4}	1.95	.025	3.10	.975
.2	7.18×10^{-4}	4.28	.030	3.00	.912
.3	4.94×10^{-4}	6.95	.040	2.88	.830
.4	-	-	-	2.68	.728
.5	-	-	-	2.48	.623

$R/a \cong 10^{-2}$

$h/L = 1/8$

$kL^{(1)}$ is the first root of (I.71)

ω_1^0 is the fundamental frequency of the corresponding uniform beam

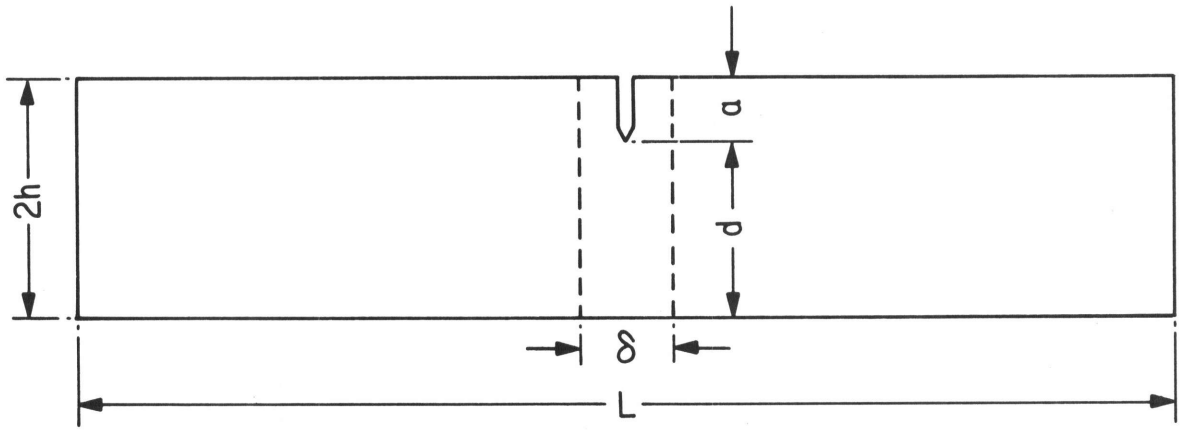

Fig. 1 - Specimen configuration

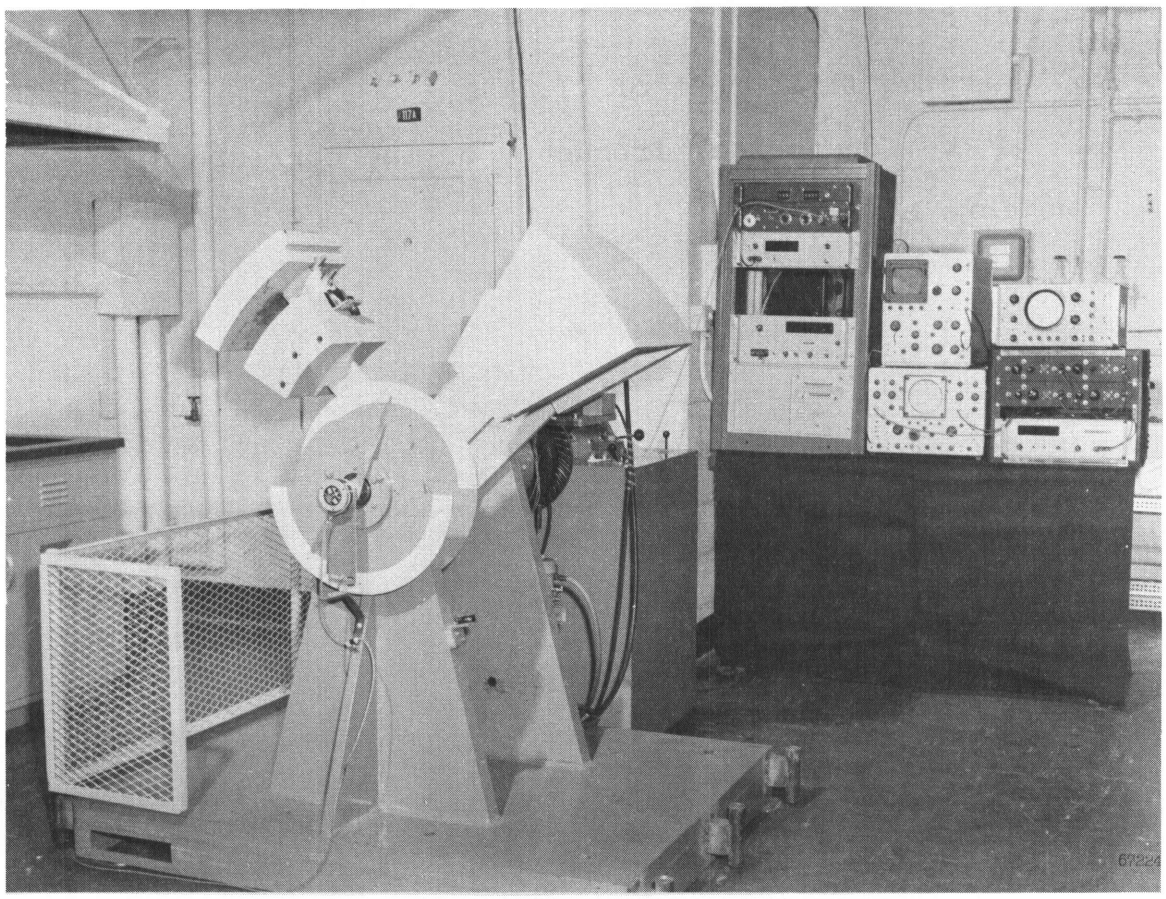

Fig. 2 - Double pendulum impact machine

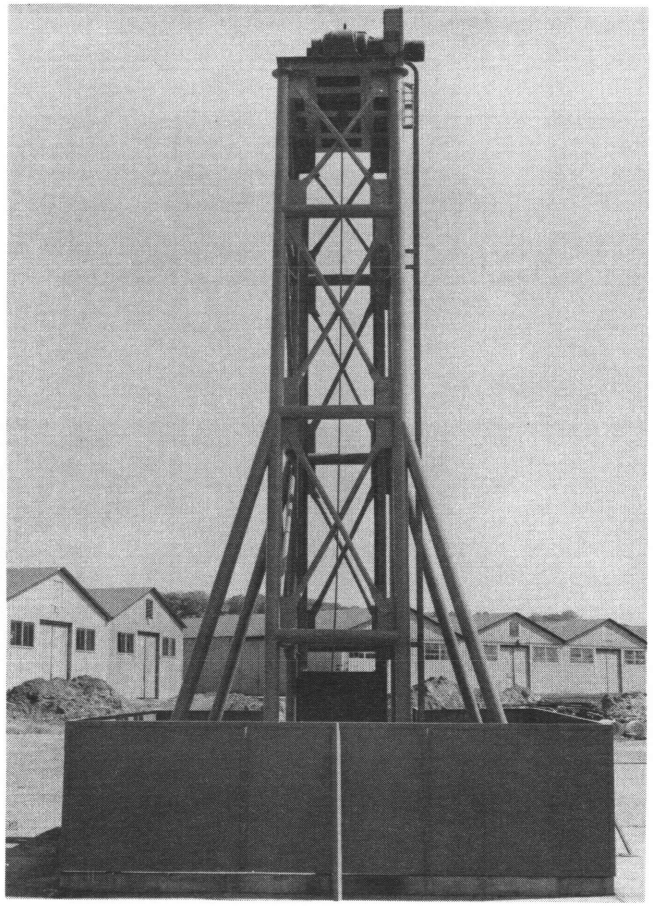

(a)

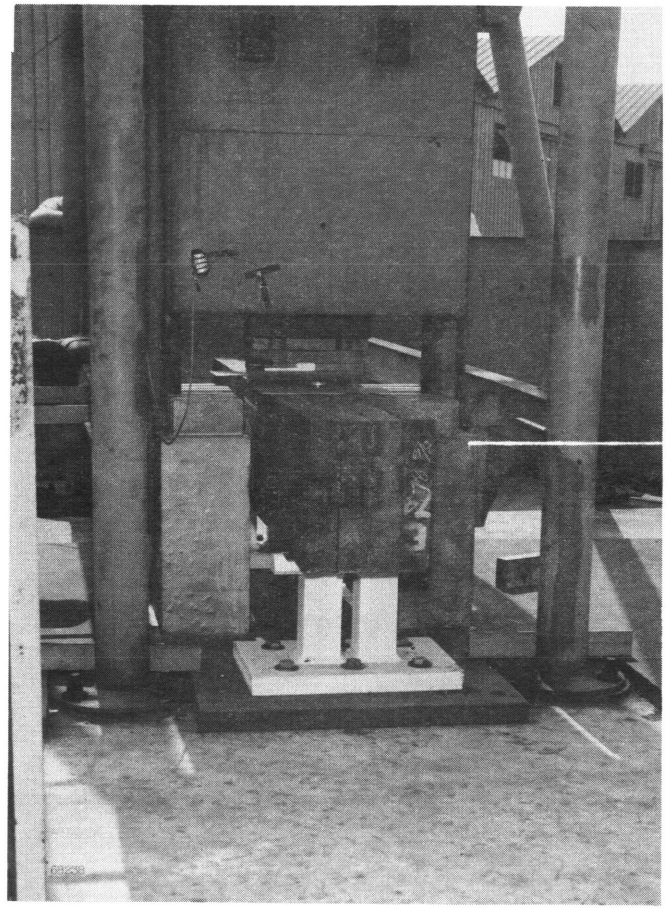

(b)

Fig. 3 - Drop-weight impact machine

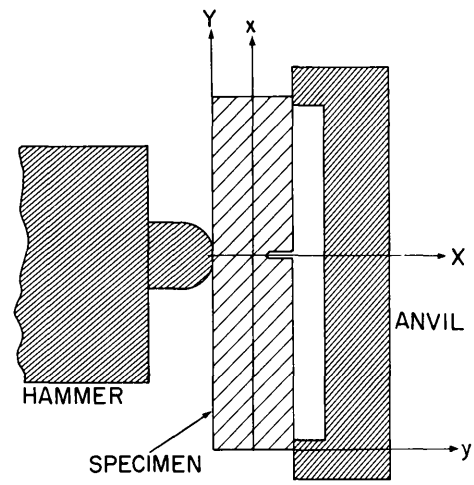

X-Y COORDINATES FIXED AT POINT OF IMPACT
x'-y' COORDINATES FIXED IN BEAM

Fig. 4 - Coordinate system

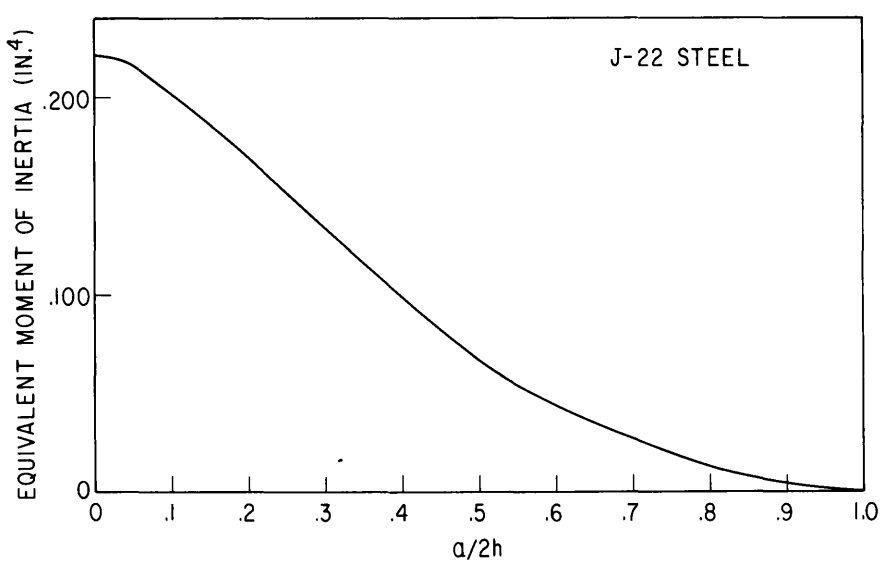

Fig. 5 - Equivalent moment of inertia vs notch depth to width ratio for the 5/8-in. DT specimen

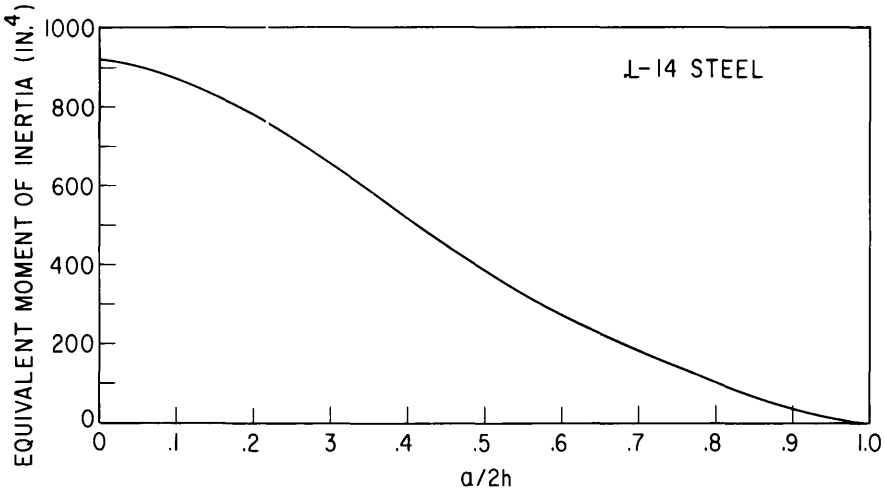

Fig. 6 - Equivalent moment of inertia vs notch depth to width ratio for the 6-3/8-inch DT specimen

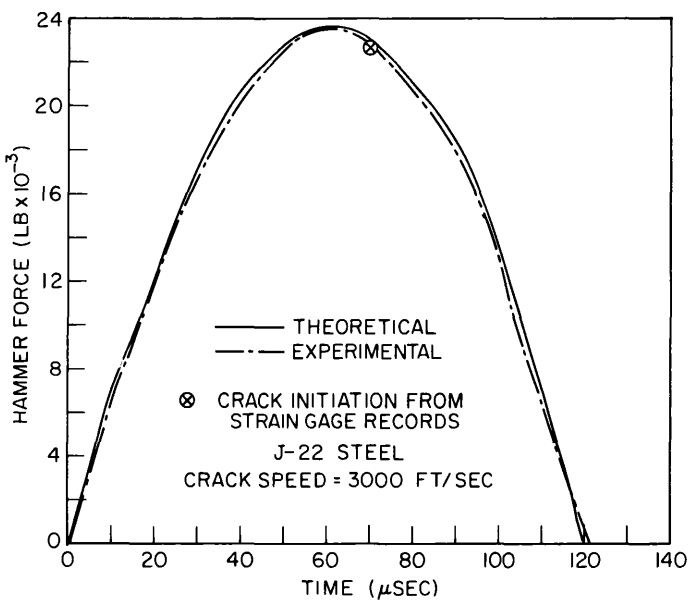

Fig. 7 - Hammer force vs time (J-22 steel)

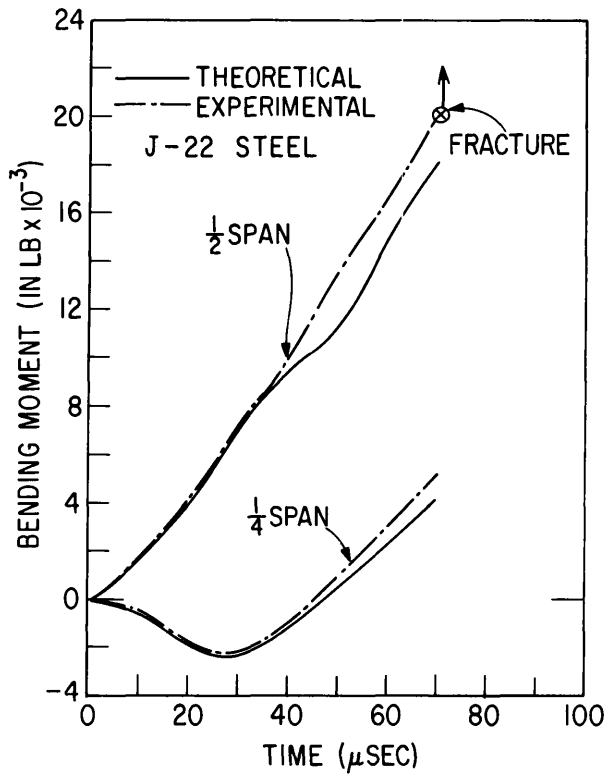

Fig. 8 - Bending moment vs time (J-22 steel)

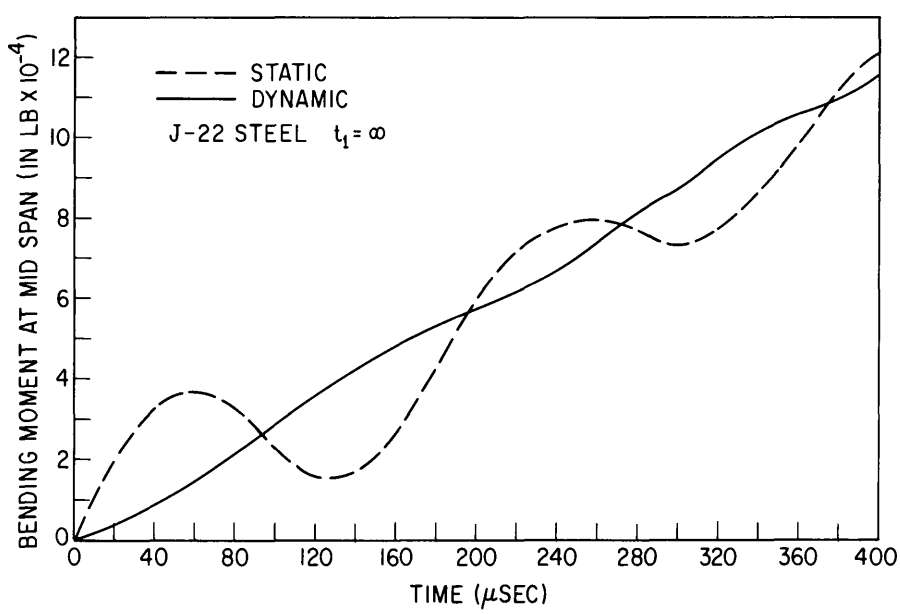

Fig. 9 - Bending moment vs time (J-22 steel, no fracture)

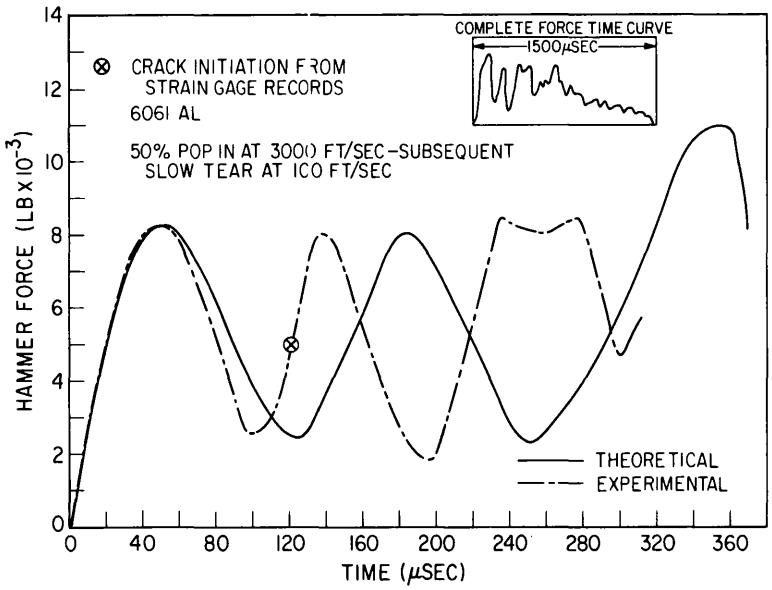

Fig. 10 - Hammer force vs time (6061 Al)

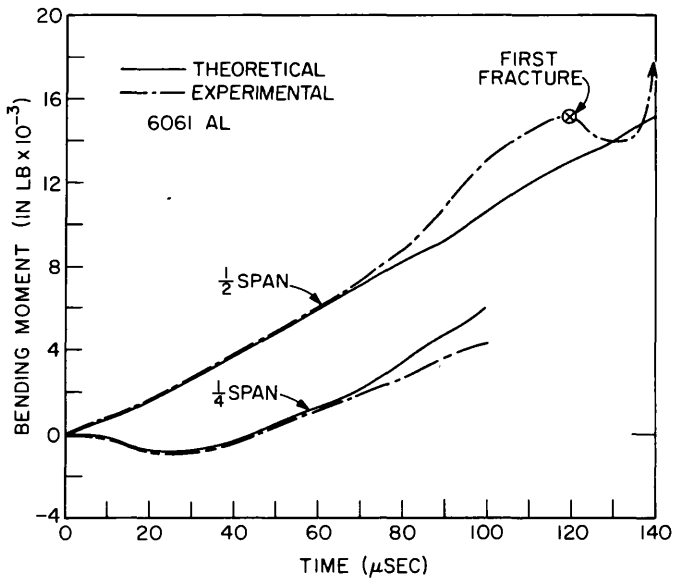

Fig. 11 - Bending moment vs time (6061 Al)

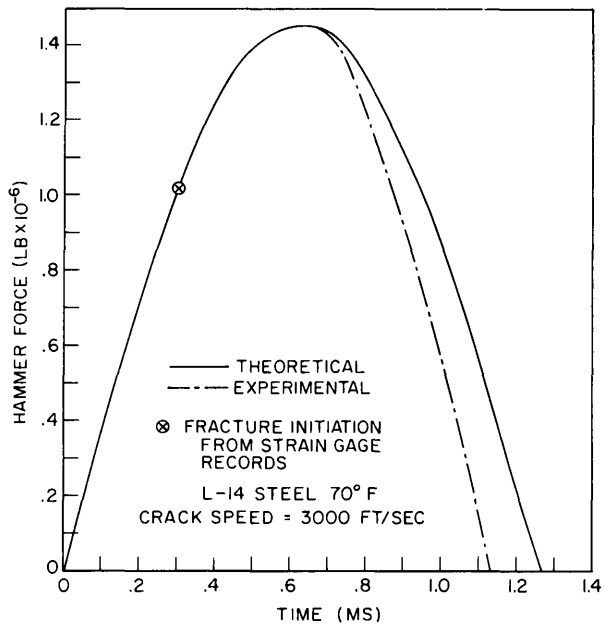

Fig. 12 - Hammer force vs time (L-14 steel, 70°F)

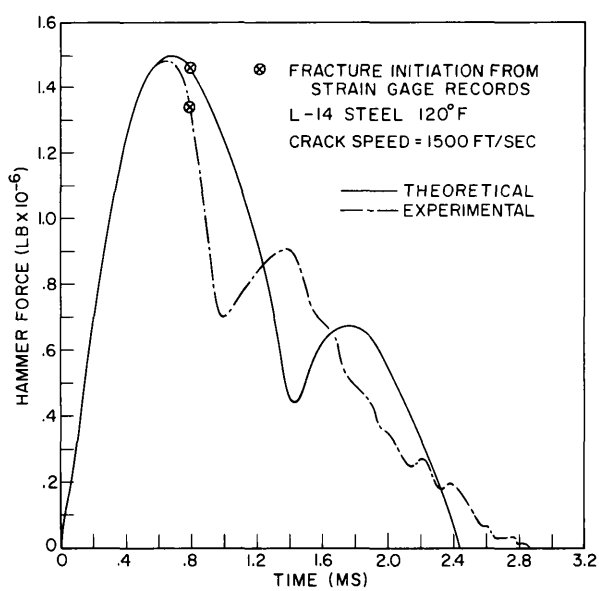

Fig. 13 - Hammer force vs (L-14 steel, 120° F)

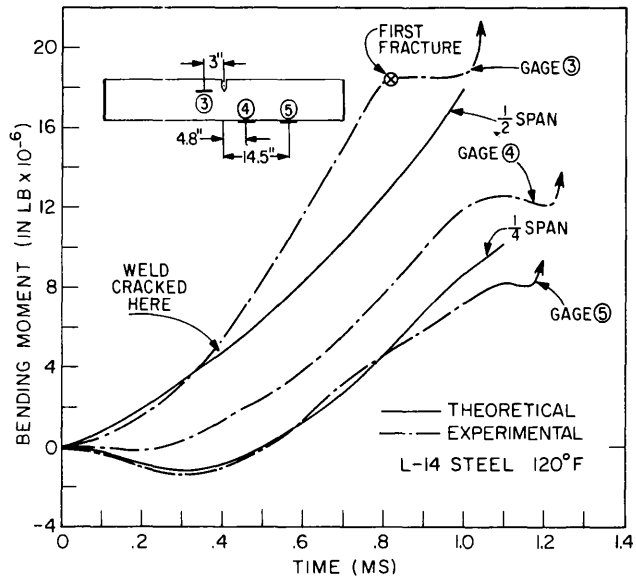

Fig. 14 - Bending moment vs time (L-14 steel, 120° F)

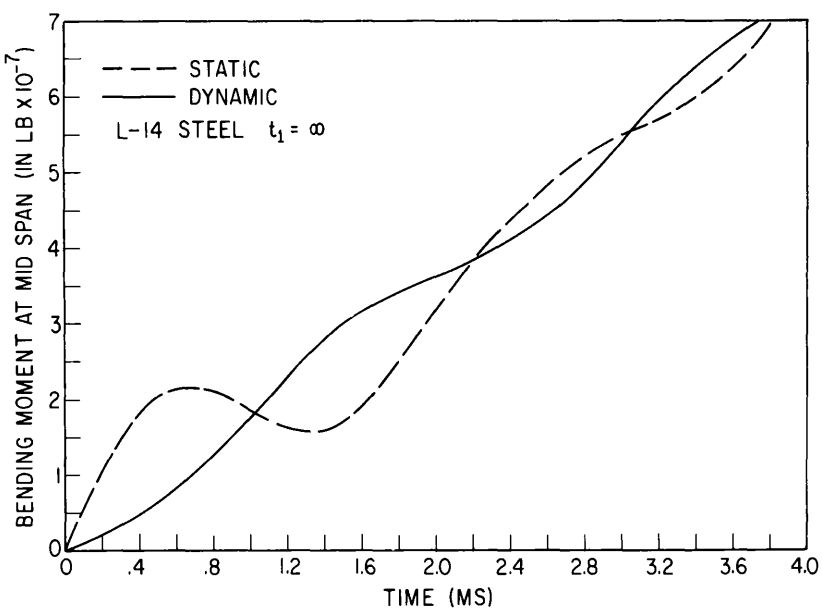

Fig. 15 - Bending moment vs time (L-14 steel, no fracture)

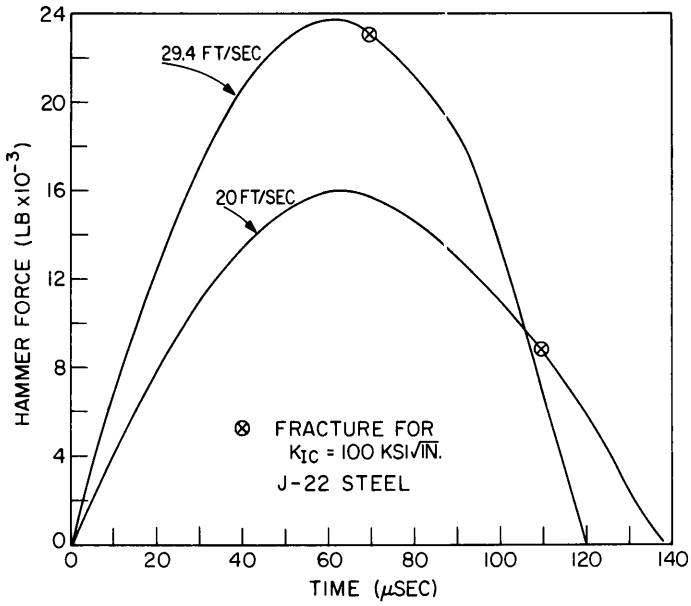

Fig. 16 - Effect of initial impact velocity on the force-time response (J-22 steel)

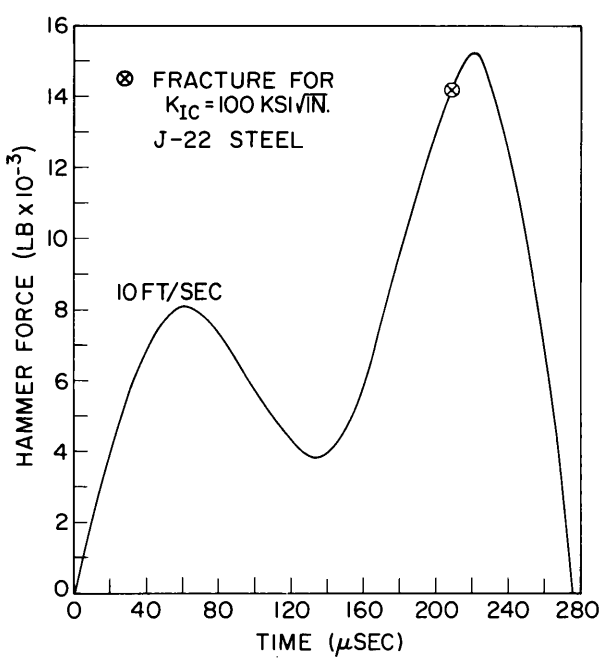

Fig. 17 - Force-time response for an initial impact velocity decreased from those of Fig. 16

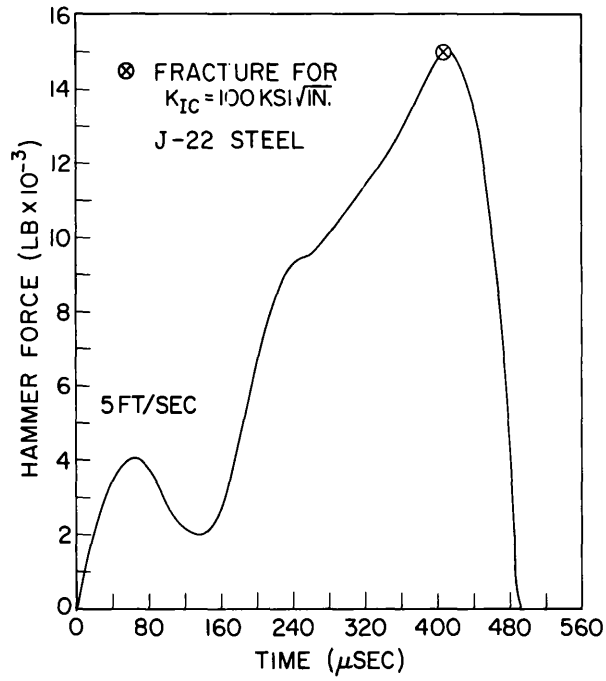

Fig. 18 - Force-time response for an initial impact velocity further decreased from those of Figs. 16 and 17

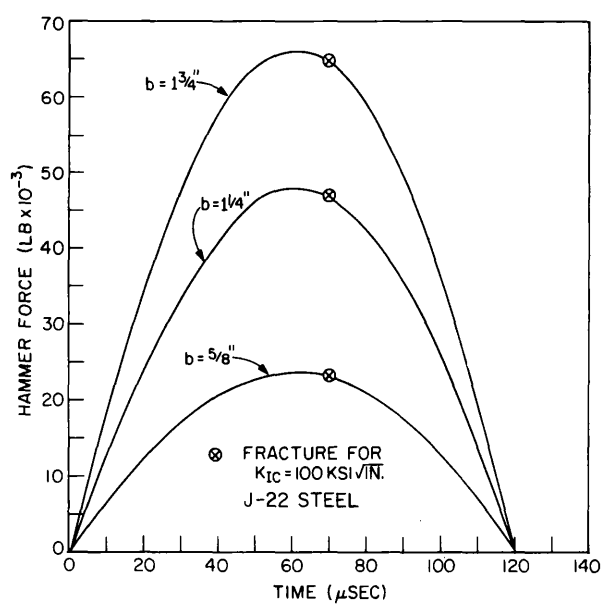

Fig. 19 - Effect of specimen thickness on the force-time response (J-22 steel)

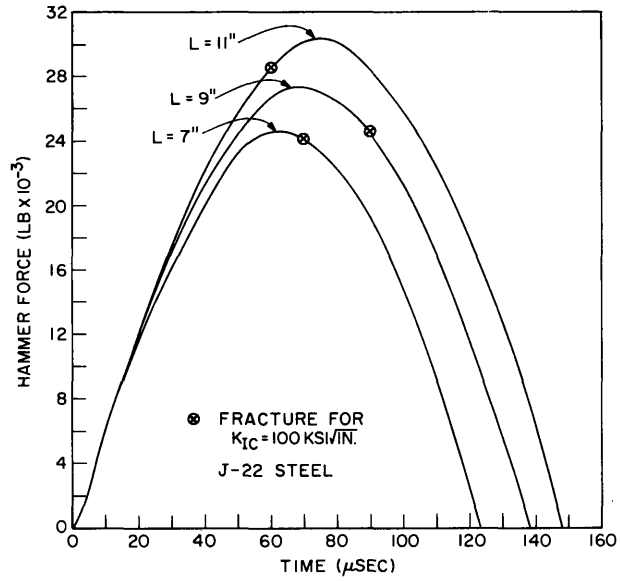

Fig. 20 - Effect of specimen length on the force-time response (J-22 steel)

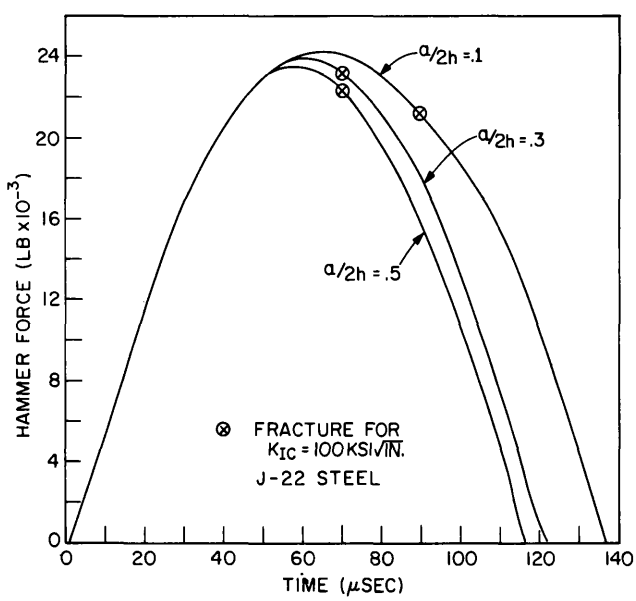

Fig. 21 - Effect of specimen notch depth to width ratio on the force-time response (J-22 steel)

Security Classification

DOCUMENT CONTROL DATA - R & D

(Security classification of title, body of abstract and indexing annotation must be entered when the overall report is classified)

1. ORIGINATING ACTIVITY *(Corporate author)* Naval Research Laboratory Washington, D.C., 20390	2a. REPORT SECURITY CLASSIFICATION Unclassified 2b. GROUP

3. REPORT TITLE

AN ANALYSIS OF THE FORCES AND BENDING MOMENTS GENERATED DURING THE NRL DYNAMIC TEAR TEST

4. DESCRIPTIVE NOTES *(Type of report and inclusive dates)*

An interim report on a continuing problem.

5. AUTHOR(S) *(First name, middle initial, last name)*

G.E. Nash

6. REPORT DATE January 30, 1969	7a. TOTAL NO. OF PAGES 72	7b. NO. OF REFS 18
8a. CONTRACT OR GRANT NO. NRL Problem M01-25 b. PROJECT NO. RR007-01-46-5432 c. d.	9a. ORIGINATOR'S REPORT NUMBER(S) NRL Report 6864 9b. OTHER REPORT NO(S) *(Any other numbers that may be assigned this report)*	

10. DISTRIBUTION STATEMENT

This document has been approved for public release and sale; its distribution is unlimited.

11. SUPPLEMENTARY NOTES	12. SPONSORING MILITARY ACTIVITY Department of the Navy (Office of Naval Research), Washington, D.C., 20360

13. ABSTRACT

An analysis is presented which predicts the hammer forees, specimen bending moments, and tear energies, generated during the NRL Dynamic Tear test. The theoretical predictions agree quite well with experimental observations for relatively brittle materials.

The tear energy per unit net area calculated from this analysis is shown to vary significantly with initial impact velocity and specimen length for a brittle material. It is relatively independent of the specimen thickness and notch depth to width ratio.

DD FORM 1 NOV 65 1473 (PAGE 1)

S/N 0101-807-6801

Security Classification

Security Classification

14. KEY WORDS	LINK A ROLE	LINK A WT	LINK B ROLE	LINK B WT	LINK C ROLE	LINK C WT
Cracking (fracturing)						
Metallurgy						
Impact, tests						
Tear tests						
NRL Dynamic Tear test						
Analysis (mathematics)						
Integral equations						
Leplace transformation						
Iteration						
Test specimens						
Fractures (materials)						
Resistance						
Dynamic response						
Predictions						
Stresses						
Bending moments						
Deflection						
Impact acceleration						
Loads (forces)						
Notched beams						
Drop hammers						

DD FORM 1 NOV 65 1473 (BACK)

(PAGE 2)

Security Classification